PNAS
www.pnas.org

Absence of carbonic anhydrase in chloroplasts affects C_3 plant development but not photosynthesis

Kevin M. Hines[a-c], Vishalsingh Chaudhari[a,b], Kristen N. Edgeworth[a,d], Thomas G. Owens[e], and Maureen R. Hanson[a,f]

[a]Department of Molecular Biology and Genetics, Cornell University, Ithaca, NY 14853, USA

[b]Equal contributions

[C]Present address: Life Sciences Testing Center, Northeastern University Innovation Campus, 147 S Bedford St, Burlington, MA 01803

[d]Present address: Plant and Microbial Biosciences, Washington University in St. Louis, MO 63130

[e]Section of Plant Biology, Cornell University, Ithaca, NY 14853, USA

[f]**Corresponding author:** Maureen R. Hanson
Email: mrh5@cornell.edu

Author Contributions:
K.M.H., V.C., K.N.E., T.G.O., and M.R.H. designed research, analyzed data and reviewed the manuscript. K.M.H., V.C., T.G.O. and K.N.E. performed experiments. K.M.H., V.C., M.R.H. and T.G.O wrote the manuscript.

Competing Interest Statement: The authors declare no competing interests.

Classification: Biological Sciences. Plant Biology.

Keywords: C3 photosynthesis, bicarbonate, carbonic anhydrase, carbon fixation, chloroplast

This PDF file includes:
Main Text
Figures 1 to 9
Supplementary Information

Significance

Carbonic anhydrase enzymes located in chloroplast stroma have been hypothesized to facilitate photosynthesis in C_3 plants because they catalyze a reaction involving bicarbonate and CO_2, a substrate of the carbon-fixing enzyme RuBisCO. To test this possibility, tobacco mutants completely lacking chloroplast stromal carbonic anhydrase activity were produced by CRISPR/Cas9 mutagenesis. The plants displayed normal photosystem II activity and CO_2 assimilation, but also abnormal development and increased ROS and stromal pH. We conclude that chloroplast carbonic anhydrase does not play a direct role in providing CO_2 for carbon fixation. Instead, as is also true in microorganisms, carbonic anhydrase is necessary to supply bicarbonate for biosynthetic processes.

ABSTRACT

The enzyme carbonic anhydrase (CA), which catalyzes the interconversion of bicarbonate with carbon dioxide (CO_2) and water, has been hypothesized to play a role in C_3 photosynthesis. We identified two tobacco stromal CAs, βCA1 and βCA5, and produced CRISPR/Cas9 mutants affecting their encoding genes. While single knockout lines *Δβca1* and *Δβca5* had no striking phenotypic differences compared to WT plants, *Δβca1ca5* leaves developed abnormally and exhibited large necrotic lesions, even when supplied with sucrose. Leaf development of *Δβca1ca5* plants normalized at 9000 ppm CO_2. Leaves of *Δβca1ca5* mutants and WT that had matured in high CO_2 had identical CO_2 fixation rates and photosystem II efficiency. Fatty acids, which are formed through reactions with bicarbonate substrates, exhibited abnormal profiles in the chloroplast CA-less mutant. Emerging *Δβca1ca5* leaves produce reactive oxygen species in chloroplasts, perhaps due to lower non-photochemical quenching efficiency compared to wild-type. *Δβca1ca5* seedling germination and development is negatively affected at ambient CO_2. Transgenes expressing full-length βCA1 and βCA5 proteins complemented the *Δβca1ca5* mutation but inactivated (ΔZn-βCA1) and cytoplasm-localized (Δ62-βCA1) forms of βCA1 did not reverse the growth phenotype. Nevertheless, expression of the inactivated ΔZn-βCA1 protein was able to restore the hypersensitive response to tobacco mosaic virus, while *Δβca1* and *Δβca1ca5* plants failed to show a hypersensitive response. We conclude that stromal CA plays a role in plant development, likely through providing bicarbonate for biosynthetic reactions, but stromal CA is not needed for maximal rates of photosynthesis in the C_3 plant tobacco.

INTRODUCTION

The metalloenzyme carbonic anhydrase (CA, EC 4.2.1.1) catalyzes the reversible hydration of carbon dioxide with bicarbonate and protons with carbonic acid as an intermediate (Fig. 1). The uncatalyzed reactions are quite slow, with effective rate constants of ~0.15 s^{-1} for the forward reaction and 50 s^{-1} for the reverse reaction; at equilibrium, dissolved CO2 is favored over bicarbonate by a factor of 340. CAs have one of the fastest catalytic cycles and increase the rate

by which carbon dioxide and bicarbonate reach equilibrium by about seven orders of magnitude (1).

Vascular land plants contain α-, β-, and γ- CAs (2), which function in a myriad of physiological roles depending on the plant and the type of photosynthesis it carries out (3, 4). In C_3 photosynthetic plants, dissolved CO_2 is the substrate for the enzyme RuBisCO, which feeds inorganic carbon into the Calvin cycle. In C_4 and Crassulacean Acid Metabolism (CAM) photosynthesis, inorganic carbon is ultimately fixed from dissolved CO_2 and RuBisCO but is initially fixed from bicarbonate via the enzyme phosphoenolpyruvate carboxylase (PEPCase) (5). Considering the location of CA function between dissolved CO_2 and bicarbonate, one might anticipate very different photosynthetic functions for CAs in C_3 versus C_4 and CAM plants (6, 7).

Research on CAs in C_3 plants has resulted in the assignment of several roles to the enzymes. The chloroplasts of *Arabidopsis thaliana* (hereafter Arabidopsis) are known to contain at least two stromal CAs: βCA1 and βCA5 (8). In Arabidopsis, the chloroplast-localized βCA1 is the most highly expressed CA in leaf tissue, with nearly 50 times the amount of RNAseq reads and 13 times the number of ESTs compared to βCA5 (9). Tobacco βCA1 is a salicylic acid (SA)-binding protein and participates in plant defense. Silencing of βCA1 in tobacco resulted in a reduction in the hypersensitive response (HR) during a *Pto-avrPto* interaction (10) and, more recently, multiple βCAs have been shown to play a role in the perception of SA in Arabidopsis (11). Mutating *both* the chloroplast-localized βCA1 and plasma membrane-localized βCA4 in Arabidopsis caused a reduction in stomatal CO_2 response (12, 13). In another study of the *βca1ca4* Arabidopsis mutant, researchers observed an intolerance to oxidative stress, suggesting that CAs play a role in cell death homeostasis during light stress (14). Transgenic tobacco plants carrying an antisense construct that reduced stromal CA expression to 5% of the wild-type level had altered lipid biosynthesis, though plant morphology appeared to be normal (15). Furthermore, cytoplasmic CAs like βCA2 may also play an important function in certain cellular biosynthesis pathways, as demonstrated in Arabidopsis *βca2ca4* mutants, which showed a significant decrease in aspartate that was rescued when plants were grown in elevated CO_2 levels (9).

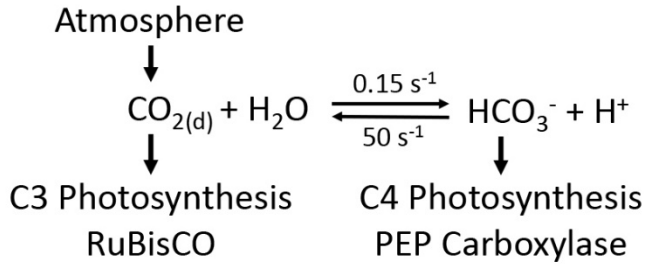

Fig. 1. Scheme illustrating carbonate equilibria, the reactions catalyzed by CA, and their coupling to the fixation of atmospheric CO_2 in C_3, C_4 and CAM photosynthesis. Rate constants are in pure water at 25°C.

Although CAs in plants can account for as much as 20% of total soluble leaf protein (3), one study has suggested a limited role of CAs in C_3 photosynthesis. In *Nicotiana tabacum* (tobacco, a

C_3 plant), reduction of chloroplast CA activity by 99% caused no significant reduction in the CO_2 assimilation rate (16). However, CAs have a very high catalytic rate, so that even as little as 1% remaining CA could potentially be adequate for many of its functions in the stroma. Nevertheless, this study suggests the possibility that most of CO_2 that enters the leaf from the atmosphere is used directly by RuBisCO without passing through a bicarbonate pool (17).

Interest in the role of stromal CAs has recently been reawakened because of efforts to install CO_2-concentrating mechanisms into C_3 plant chloroplasts (18, 19). In cyanobacteria, CA is located within the carboxysome, where bicarbonate is converted to CO_2 for use by RuBisCO (20, 21). If CA is introduced by transgene expression into the cyanobacterial cytoplasm, the CO_2-concentrating mechanism cannot function (21). Incorporating an operational carboxysome within chloroplasts will require removal of all CA in the stroma (22), which is the functional equivalent of the cytoplasm of cyanobacteria. However, the consequences of a complete lack of stromal CA activity have not previously been investigated in vascular plants.

Here we identify βCA1 and βCA5 as the tobacco chloroplast stromal CAs and use the CRISPR/Cas9 system to generate knockout lines, thus removing all CA activity from the stroma. We discovered that the absence of stromal CA activity had unexpected detrimental effects on leaf, floral bud and seed development and increased the reactive oxygen species and increased the stroma pH. We demonstrate that the developmental phenotypes can be reversed by growing the mutant plants in high (9000 ppm) CO_2, which is known to result in increased non-enzymatic production of bicarbonate. Importantly, measurements of photosynthesis and gas exchange did not distinguish the double mutant from wild-type, indicating that rapid equilibration of dissolved CO_2 and bicarbonate pools is not required for high steady-state rates of C_3 photosynthesis.

Results

Tobacco CA enzymes βCA1 and βCA5 localize to the chloroplast stroma. The coding sequences (CDS) of 3 candidate tobacco CA genes were selected based on TargetP sequence-based predictions (βCA1 and βCA5) and previous localization studies of CA homologs in Arabidopsis (αCA1). A series of YFP fusion experiments were carried out to determine which of these tobacco CA enzymes localize to the chloroplast stroma. In Arabidopsis, βCA1 and βCA5 have been observed to localize to the chloroplast stroma (8). βCA1 in Arabidopsis and tobacco are 75-76 % similar and the βCA5 proteins are 78-83% similar.

Tobacco YFP-fused βCA1 and βCA5 were both found to be localized to the chloroplast stroma (Fig. 2A). There are 4 predicted isoforms for βCA5 in tobacco (Accession numbers XP_016482110, XP_016482109, XP_016446542, and XP_016446541), two for each of the two tobacco progenitor *N. sylvestris* and *N. tomentosiformis* alleles, but reverse transcription of tobacco leaf RNA yielded only 1 isoform for each (see Methods).

The tobacco αCA1 is predicted to be a secretory pathway protein with a transmembrane sequence near the N-terminus, but it is reported to be localized to the chloroplast stroma in Arabidopsis (23). YFP-fused tobacco αCA1 did not localize to the chloroplast stroma and instead appeared to be on the plasma membrane, which is consistent with a software prediction (*SI Appendix*, Fig. S1). Taken together, YFP localization indicates that βCA1 and βCA5 are the CA enzymes in the stroma of tobacco chloroplasts.

Targeting tobacco βca1 and βca5 with CRISPR/Cas9. The CRISPR/Cas9 system was used to generate mutations in the tobacco βca1 and βca5 genes to create three transgenic lines: Δ*βca1,* Δ*βca5,* and the double knockout Δ*βca1ca5*. Tobacco is an allotetraploid (a hybrid of *Nicotiana*

sylvestris and *Nicotiana tomentosiformis*), so there are two homologs for each of the CA genes. The sgRNAs were designed to target the sequences of both forms of the CA homologs (*SI Appendix*, Fig. S2).

A Δβ*ca1* mutant line contains a 2 bp deletion in the mRNA sequence of one homolog of the βca1 gene and a 52 bp deletion in the other (*SI Appendix*, Fig. S3). Both deletions created a frame-shift mutation, resulting in an early stop codon in the coding sequences. A Δ*βca5* mutant contains 2 bp and 31 bp deletions in the mRNA sequence of the two βca5 homologs, both of which result in frame-shift mutations. The βca1 homologs in the double mutant Δ*βca1ca5* comprise of a 1 bp insertion or a 2 bp deletion and the βca5 homologs both have large, 31 bp deletions between the two sgRNA target sites (*SI Appendix*, Fig. S3). The sequencing data demonstrates the creation of frame-shift mutations in the targeted CA genes in all the CRISPR/Cas9-generated transgenic lines.

The gross morphology of Δβ*ca1* and Δβ*ca5* is similar to WT tobacco when the plants are grown at ambient CO_2 concentrations (Fig. 2B). In contrast, Δ*βca1ca5* displays a dramatic developmental phenotype, which results in pale and shriveled leaves. The plants in Fig. 2B were first grown at 9000 ppm CO_2 for 4 weeks before being transferred to ambient CO_2 for two weeks and then imaged. The white arrows highlight Δ*βca1ca5* leaves which developed in high CO_2 before being transferred.

Carbonic anhydrase activity in mutant lines. The CA activity of the lines was measured in whole leaf homogenate from plants growing at ambient CO_2 in 16hr daylight, using leaves which had expanded under high CO_2 conditions. We used the CA activity assay described in (11) with modifications (see Methods). This assay measures the activity of CAs in all subcellular locations of the tissue used, not only activity within the chloroplasts. Δ*βca1* and Δ*βca1ca5*, the two lines in which βCA1 was mutated, show greatly decreased levels of CA activity (Fig. 2C), while CA activity in Δ*βca5* showed no reduction. As expected, most of the CA activity found in leaves appears to come from the highly expressed βCA1 enzyme, with the Δ*βca1* transgenic line showing an 87% reduction in CA activity compared to WT (Fig. 2C).

Morphological characteristics of *Δβca1ca5* transgenic tobacco. The gross morphological and developmental phenotypes of the *Δβca1ca5* double mutant were observed at ambient CO_2 concentrations (about 415 ppm; Figs. 2B and 3). When *Δβca1ca5* mutants were transplanted into soil and grown in 9000 ppm CO_2, their morphology (leaf color and form) appeared to mirror WT tobacco (Fig. 3B). Leaves of *Δβca1ca5* that were able to fully expand at high CO_2 retained their WT-like morphology when they were transferred back to ambient CO_2 concentrations (Fig. 3C, green arrow). These leaves did not become necrotic and remained green as the plant transitioned into flowering. Leaves that did not finish expanding in high CO_2 displayed necrotic lesions in their still-developing photosynthetic tissues (Fig. 3C, blue arrow) and leaves that had initiated their development in ambient CO_2 also exhibited the mutant phenotype (Fig. 3C, red arrow and Fig. 3D). When first emerging at ambient CO_2 concentrations, *Δβca1ca5* leaves do not show any obvious phenotypes or gross morphological differences from WT (Fig. 3G, leaf 1). As leaf development progresses, however, necrotic lesions form and spread throughout the photosynthetic tissue. The midrib and primary veins do not display a cell-death phenotype (Fig. 3G, leaves 6 and 7). Despite the death of mesophyll cells, the leaves remain attached to the stem of the tobacco plants. The pattern of necrosis (appearing first at the base, Fig. 3D and Fig. S5)

matches the pattern in which leaves transition from sink-to-source tissue (tip to base) (24). This pattern is consistent with the lack of necrosis in tissues like the midrib and primary veins.

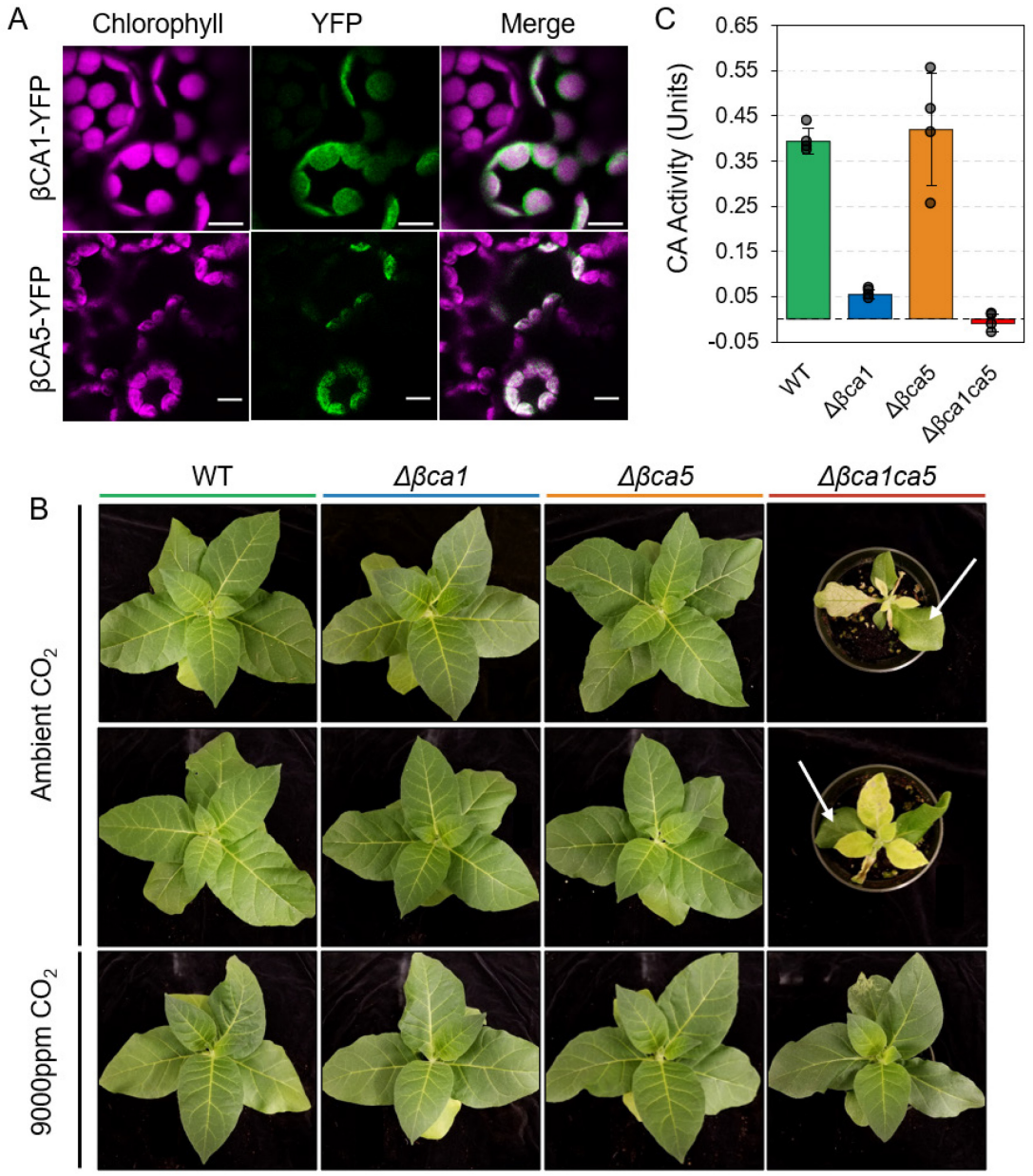

Fig. 2. Localization and CRISPR-generated mutations of tobacco chloroplast CAs. (A) Confocal imaging of CA-YFP constructs transiently expressed in *N. tabacum* mesophyll cells. βCA1-YFP localized to the chloroplast stroma and cytoplasm. βCA5-YFP localized to the chloroplast stroma. Magenta: Chlorophyll autofluorescence, excitation 633nm. Green: YFP, excitation 514nm. Bars=10μm. (B) Single mutant lines *Δβca1* and *Δβca5* show no observable phenotype in their gross morphology compared to WT. The double mutant, *Δβca1ca5* produces pale leaves with symptoms of necrosis. Plants were grown in 9000 ppm CO_2 for 4 weeks and then transferred to ambient CO_2 for 2 weeks before being imaged. White arrows indicate *Δβca1ca5* leaves that developed in high CO_2. (C) CA activity of whole leaf homogenate at ambient CO_2

(Bars: standard error). There is no significant difference detectable between WT activity and *Δβca5* activity, with 4 replicates for each assay (*t*-test, p=0.68), while *Δβca1* and *Δβca1ca5* differ with p=.0001 (*t*-test).

At ambient CO_2, *Δβca1ca5* plants also exhibit a unique flowering phenotype. Before the emergence of petals, the developing flower buds experience an early termination event, separating from the stem at the abscission zone (Figs. 3E and 3F). A small number of buds eventually develop into mature flowers at ambient CO_2 and produce seeds via natural self-pollination.

Free fatty acid distribution is different between WT and *Δβca1ca5* leaves. Previously, acetyl incorporation into lipids, which is catalyzed by acetyl-CoA carboxylase using bicarbonate as a substrate, was found to be reduced in antisense βCA1 tobacco in which CA was present at only 5% of wild-type levels (15). Here we investigated the free fatty acid (FFA) makeup of WT and Δ*βca1ca5* leaves (one young leaf from each of the first three nodes) grown on sucrose media in ambient CO_2. Five fatty acid classes were detected by mass spectroscopy (Fig. 4A and *SI Appendix,* Fig. *S4*). A significant difference between the two lines was observed. Unsaturated FFAs 18:2, 18:3, and 18:4 were upregulated in Δβ*ca1ca5* leaves whereas saturated FFAs 16:0 and 18:0 were higher in WT leaves. Overall, the total area under the peak for measured fatty acids was lower by about 30% in Δβ*ca1ca5* when compared to WT.

Seed development and germination is severely affected in Δβca1ca5. Given that bicarbonate is required for fatty acid synthesis, a reduction in its availability due to the absence of stromal CA would be expected to affect synthesis of lipids in embryos and seeds. Earlier, Hoang and Chapman (15) reported that inhibitors of CA affected incorporation of acetyl into lipids in cotton embryos. We investigated the effect of a complete absence of CA in the tobacco mutant on seed filling and germination.

Seeds produced by *Δβca1ca5* in ambient CO_2 had significant morphological alterations and often contained large indentations in their coats, while the morphological phenotype of seeds from high CO_2-grown *Δβca1ca5* plants is similar to WT (Fig. 4B). The high CO_2 *Δβca1ca5* plants produced heavier seeds, averaging 0.068mg/seed compared to a mass of 0.038mg/seed produced from plants in ambient CO_2 (Fig. 4C). In both atmospheric conditions, however, the mutant seeds weighed less than WT seeds (p=0.00002 and p=0.0007 for low and high CO_2 respectively, *t*-test), which had an average mass of 0.081 mg, indicating the 9000 ppm CO_2 growth could not completely restore biosynthetic reactions utilizing bicarbonate. To observe whether both mass and seed size differed, the two-dimensional areas of WT and *Δβca1ca5* seeds were measured. The seeds from ambient CO_2-grown mutants had an average area of 0.29 mm^2, which was a statistically significant difference compared to the WT seed area of 0.32 mm^2 (Fig. 4D, p= 0.0002, *t*-test). There was no significant difference in the average area of WT seeds 0.32 mm^2 compared to the seeds of 9000 ppm CO_2 grown *Δβca1ca5* plants, at 0.32 mm^2 and 0.31 mm^2 respectively (Fig. 4D, p=0.52).

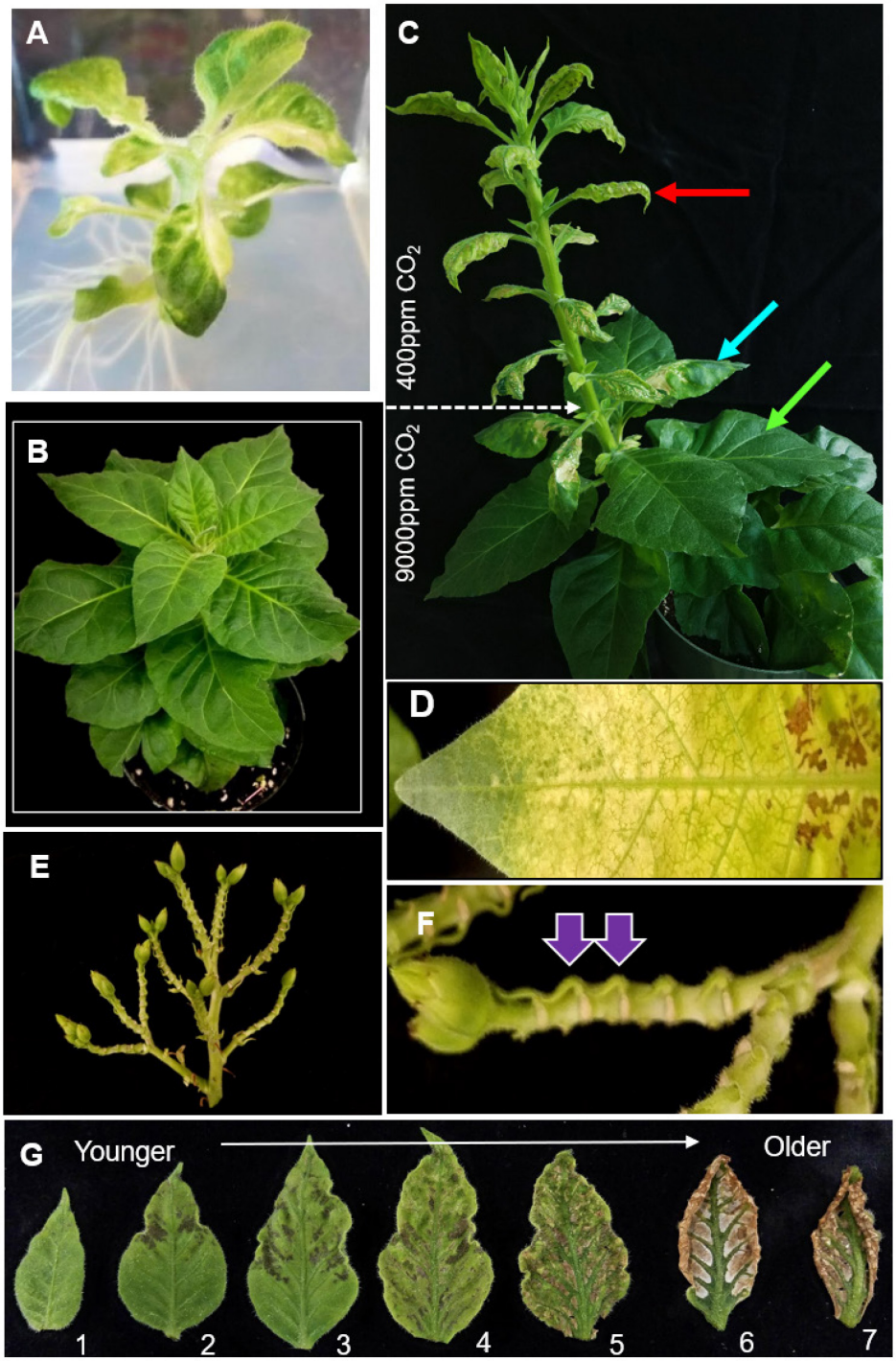

Fig. 3. *Δβca1ca5* mutants have a severe developmental phenotype rescued by high CO_2. (A) *Δβca1ca5* shoot at ambient CO_2 growing on 3% sucrose media. (B) *Δβca1ca5* transplanted to soil and grown at 9000 ppm CO_2. (C) *Δβca1ca5* mutant allowed to mature for 4 weeks at 9000 ppm CO_2 before being transferred to ambient CO_2 (at white arrow) and allowed to grow for 4 more weeks. Green arrow: Example of a leaf that fully expanded at high CO_2. Blue arrow: leaf that was developing at the time of transfer. Red arrow: leaf that budded and developed at ambient CO_2. (D) An expanding high-CO_2-grown *Δβca1ca5* leaf after being transferred to

ambient CO_2. (E & F) Abscission of flowering buds in *Δβca1ca5* mutants at ambient CO_2. Purple arrow shows two of the abscission zones. (G) Development of mutant phenotype in leaves developing at ambient CO_2 (left to right: youngest to oldest). Numbers indicate node position from the top of the plant.Seeds from *Δβca1ca5* plants produced in high CO_2 resulted in substantial improvement in seed germination rates, regardless of the CO_2 concentration in which the seeds were sowed. When grown on soil, these seeds had a 72% germination rate at ambient CO_2 and a 67% germination rate at high CO_2 (Fig. 4E). Seeds produced by the *Δβca1ca5* plant grown at ambient CO_2 had germination rates of 29% and 22% when sown in soil and placed in 415 ppm CO_2 and 9000 ppm CO_2 concentrations, respectively. When placed on 3% sucrose media at 415 ppm CO_2, the seeds from low CO_2-grown *Δβca1ca5* plants had a germination rate of 28% (Fig. 4E). Thus, the growth conditions of the T0 *Δβca1ca5* parent had a strong influence on the germination rate of the ensuing seeds. Restoration of bicarbonate amount at 9000 ppm evidently provided sufficient substrate for biosynthesis in developing embryos and seeds.

The germination rates of T1 seeds from the two single knockout lines, *Δβca1* and *Δβca5*, and the double mutant *Δβca1ca5*, all produced in plants grown at ambient CO_2 (as in Figs. 3D and 3E), were measured in soil under ambient CO_2 concentrations and a long day (16h) photoperiod (Fig. 4E, F). After 7 days, 97% of *Δβca1* seeds and 100% of WT seeds germinated. Germination of seeds from *Δβca5* was delayed, with 74% of seeds germinating by day 7, and 90% by day 13. Only 3% of *Δβca1ca5* seeds germinated after 7 days; 15 days were required for the seeds to reach a germination rate of 29%.

The T1 *Δβca1* and *Δβca5* seedlings continued to develop normally under ambient CO_2 after germination (like their T0 parents). In contrast, the growth and development of T1 *Δβca1ca5* seedlings in ambient CO_2 arrested shortly after germination (Fig. 4G), irrespective of whether seeds developed in high CO_2 or ambient. Notably, the *Δβca1ca5* seedlings (Fig. 4G) failed to produce true leaves at ambient CO_2, even when grown on media containing 3% sucrose.

CA mutants show no difference in photosynthetic capacity. Chloroplast CA has long been hypothesized to play a role in provision of dissolved CO_2 for RuBisCO. If true, then such a role would likely be most pronounced when demand for CO_2 is highest, during photosynthesis at saturating light. To study the effect of removing CA from the chloroplast stroma, we imaged *in vivo* chlorophyll fluorescence from whole plants as leaves made the transition from limiting (7 μmol photons m^{-2} s^{-1}) to saturating (790 μmol photons m^{-2} s^{-1}) light. Because leaf development in the *Δβca1ca5* double mutant is severely compromised, all measurements were made on intact, fully expanded leaves from plants grown at 9000 ppm CO_2 and transferred to ambient CO_2 for 24 h before measurement. Φ_{PSII}, the efficiency with which absorbed photons are used to drive PS II electron transport, was measured at one-minute intervals beginning 10 seconds after the transition to saturating light. We observed that the kinetics of changes in Φ_{PSII} following the transition from limiting to saturating light (Fig. 5A) were nearly identical in WT, *Δβca1* and *Δβca1ca5* mutants, indicating that photosynthesis was not impaired in these mutants compared to WT. The values of Φ_{PSII} were consistently about 10% lower in the *Δβca5* mutant than in the other three genotypes.

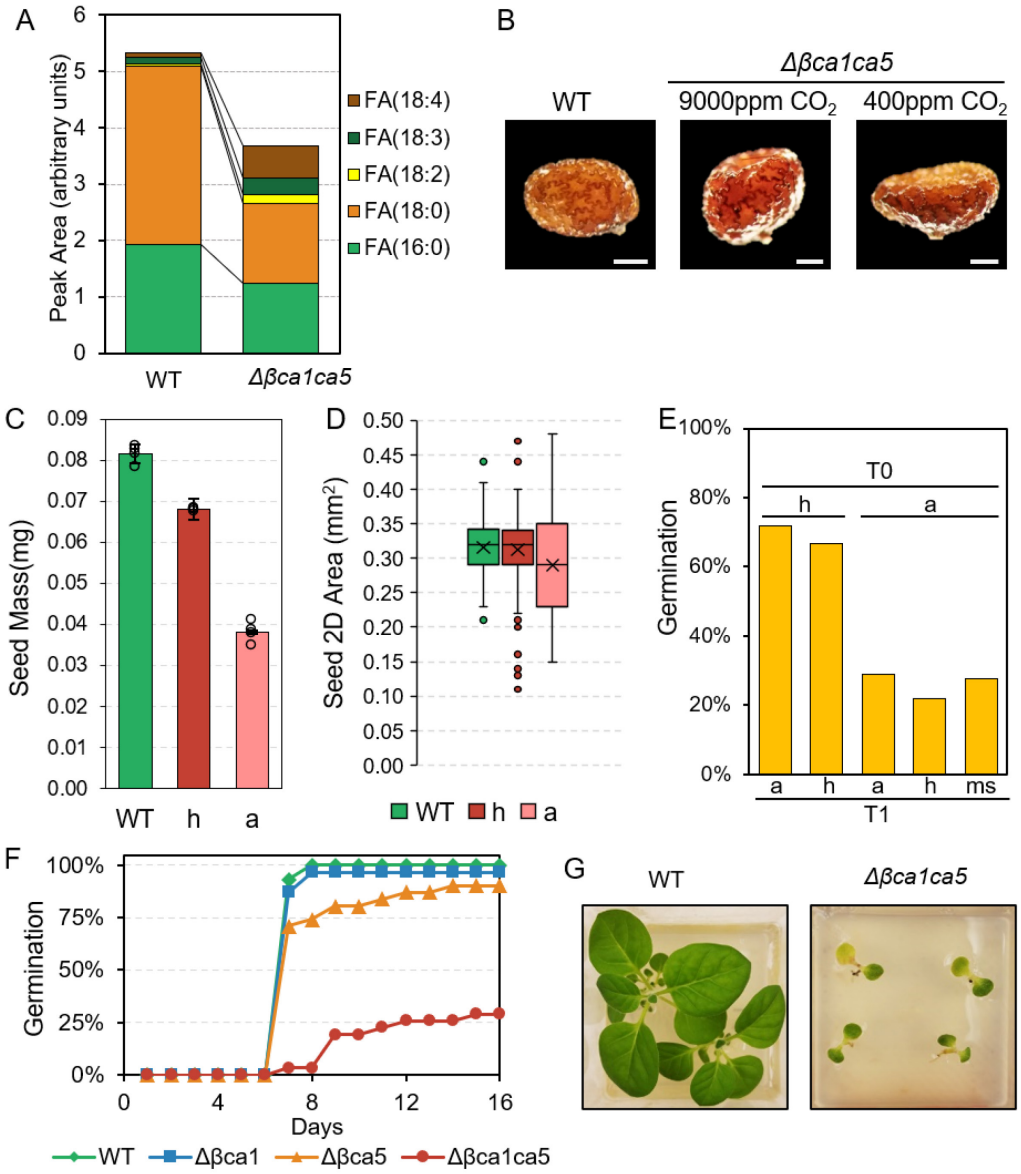

Fig. 4. Analysis of CA mutant seeds. (A) Free Fatty Acid (FFA) analysis on ambient CO_2-grown leaves of WT tobacco and the Δ*βca1ca5* mutant line ($p \leq 0.001$). Nomenclature for FFA is number of carbons::number of saturated bonds. (B) Sample comparison of T1 *Δβca1ca5* seeds with different growth conditions of the T0 mutant flowers. Bars= 0.2mm. (C) Average mass of seeds from WT and *Δβca1ca5* plants grown under high or ambient CO_2 concentrations (bars= standard deviation). (D) Average size of seeds produced by WT and *Δβca1ca5* plants grown under high or ambient CO_2 concentrations (bars=standard error). (E) Germination rate of T1 seeds derived from *Δβca1ca5* T0 plants grown in different conditions. X axis indicates germination conditions a=ambient in soil, h= high CO_2 in soil, ms = ambient in sucrose media. Top letter a or h indicates conditions during seed development. (F) Germination rates of WT seeds and T1 *Δβca1, Δβca5, and Δβca1ca5* seeds in soil at 400 ppm CO_2. Each point represents 31 seeds placed in soil (For C-E: h=9000 ppm CO_2, a=400 ppm CO_2, ms=sucrose media). (G) WT and T1 *Δβca1ca5* seedlings (from T0 grown in ambient), of the same age post sowing, on 3% sucrose media in 400 ppm CO_2. Data for (C) and (D) come from 1161 WT seeds, 838

high CO_2 *Δβca1ca5* seeds and 238 ambient CO_2 *Δβca1ca5* seeds Under optimal photosynthetic conditions, there is a complementary relationship between the yields of photochemical (Φ_{PSII}) and non-photochemical (Φ_{NPQ}) quenching, with the sum of the two being equivalent to the dark-adapted value of $F_v/F_{m\,(25)}$. While there were no significant differences among Φ_{PSII} values measured at light saturation between the mutants and WT tobacco, there was a significant decrease in Φ_{NPQ} in the Δβ*ca1ca5* double mutant (Fig. 5B).

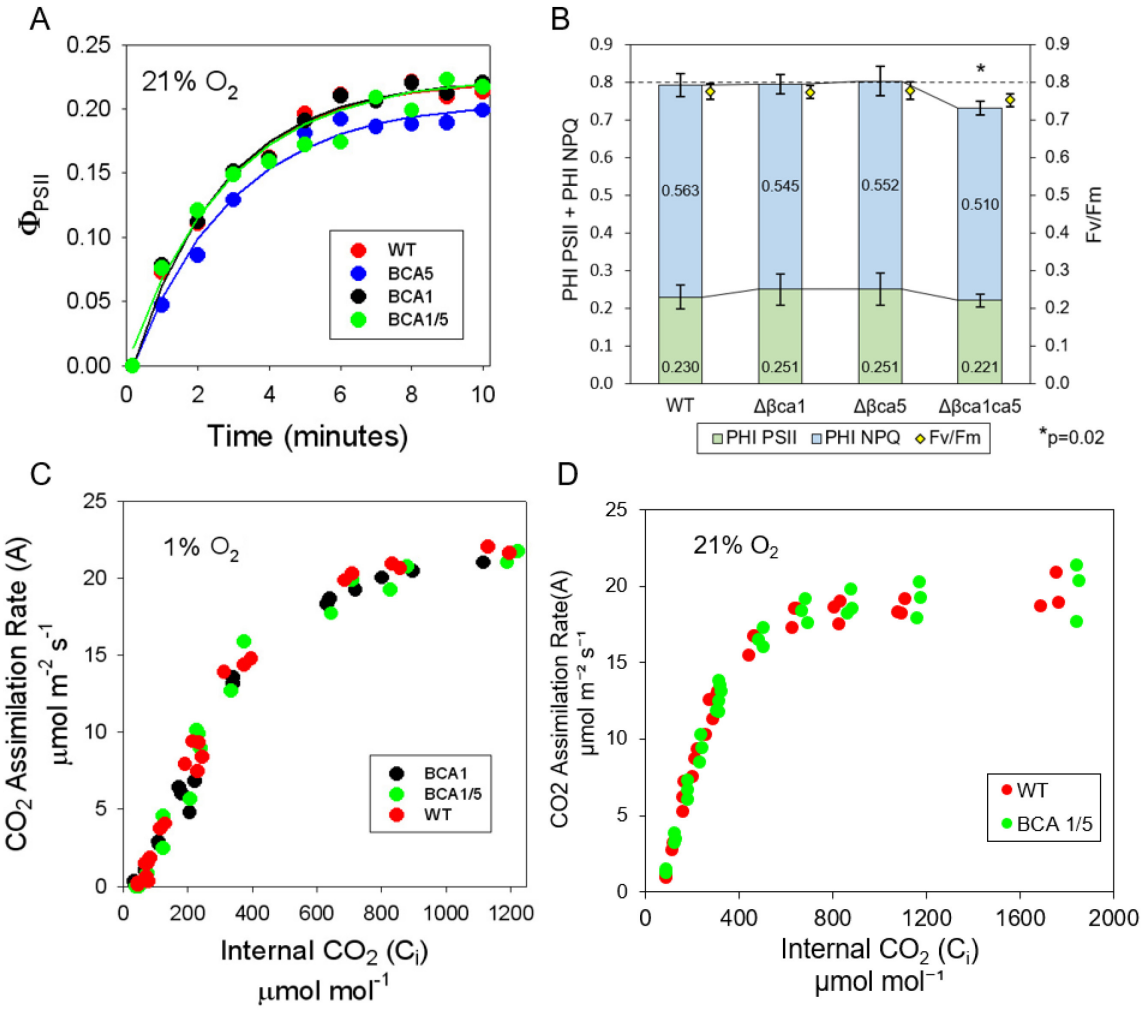

Fig. 5. Photosynthetic measurements. (A) Kinetics of PHI_{PSII} changes in response to a transition from steady state low light (7 µmol photons m^{-2} s^{-1}) to saturating light (790 µmol photons m^{-2} s^{-1}). Data are averages over 18-60 AOIs per genotype; fits are to a single exponential rise (r^2= 0.987, 0.951, 0.969, and 0.978 for WT, *Δβca1, Δβca5* and *Δβca1ca5* respectively). X-axis is minutes after transitioning to a saturating light intensity. (B) Left axis: PSII and NPQ efficiency (phi) between WT and mutant tobacco lines grown in high (9000 ppm) CO_2 for 6 weeks. The reduction in NPQ in the double mutant Δβ*ca1ca5* when compared to WT tobacco is significant (*p=0.02, student *t*-test). Right axis: Fv/Fm values show no significant difference between the 4 lines. The nominal Fv/Fm value of 0.8 is shown as a dotted line. Error bars = standard deviation. (C, D) A/C_i curves measured at 1% O_2 and ambient O_2. For 1% O_2, data are from one leaf from four different plants in each genotype. Ambient data is from 3 plants for each WT and double mutant.

Φ_{PSII} measures the fraction of absorbed photons that are used to drive total electron transport through PS II. Although a useful indicator of PS II activity and total photosynthesis, it is subject to two types of errors. In all plants, measurement of Φ_{PSII} assumes that all incident photons are absorbed, or that at least a similar fraction of incident photons are absorbed among the samples being compared. In C_3 plants, there is the further complication that a significant fraction of electron flow through PS II can be due to photorespiration rather than net CO_2 fixation, particularly under light-saturated conditions (26). To eliminate these potential errors, we measured CO_2 uptake under saturating light with O_2 reduced to 1% which eliminates photorespiratory losses without affecting photosynthesis (27). The assimilation rate (A) versus internal CO_2 (C_i) curves exhibit very similar behavior for WT and the *Δβca1* and *Δβca1ca5* mutants (Fig. 5C). This relationship was also observed at ambient O_2 (Fig. 5D). Importantly, A/C_i measurements did not distinguish WT and the double mutant at either ambient or saturating CO_2 (Fig. 5D; *SI Appendix*, Fig. S5), indicating that photosynthesis was not affected when CA activity is eliminated from the chloroplast stroma.

pH is increased in *Δβca1ca5* chloroplasts. In humans, CA plays a crucial role in the blood's bicarbonate buffer (28), and while plant CAs have been hypothesized to play a role in regulating the pH of the chloroplast stroma (29), the level of bicarbonate at equilibrium in the stroma might be too low (~1 mM at equilibrium) for it to act as an effective buffer system (2). To investigate possible changes in pH in the CA mutant lines, the pH sensitive GFP pHluorin2 was altered with the addition of a chloroplast transit peptide (from the Arabidopsis RecA protein) to its N-terminus (*SI Appendix*, Fig. S6). This construct was then transiently expressed in WT and mutant CA plants grown at ambient CO_2 and observed to localize in chloroplasts (Fig. 6B) While the exact pH cannot be determined with this method, it can give insights into the relative stromal pH of the mutants compared to the WT, which is expected to have a stromal pH of ~8 (30).

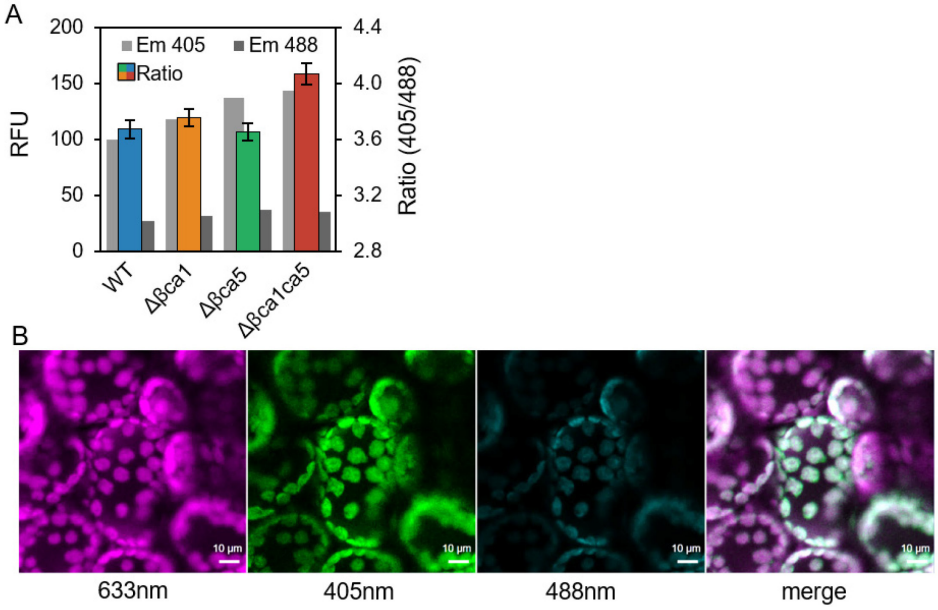

Fig. 6. Chloroplast stromal pH. (A) Ratio (colored bars) of RecAcTP-pHlourin2 signals excited by 405 nm (light grey) and 488 nm (dark grey) lasers measured on a confocal microscope. Emission signals measured in relative fluorescent units ranging from 0-255. Bars=Standard error. (B) Confocal images of chloroplast-targeted pHlourin2 in transformed WT tobacco. 633 nm: Chlorophyll A autofluorescence. 405 nm: pHlourin2. 488 nm: pHlourin2. Bars = 10 μm. The

ratio between the emission signals of pHluorin2 excited with the 405nm laser and the 488nm laser (405/488) was used to determine the relative pH (31). A high 405nm/488nm ratio observed in WT chloroplasts indicates a basic environment, which is consistent with the predicted WT stromal pH of about 8 (Fig. 6A). The pH of the single mutant lines *Δβca1* and *Δβca5* were similar to WT, but *Δβca1ca5* showed an increase in the 405/488 ratio, indicating a higher pH and more basic cellular environment in the chloroplast stroma of the mutant growing in ambient CO_2 than wild-type (Fig. 6A). The altered pH could have an effect on catalysis by enzymes whose pH optimum is less basic, further disturbing biosynthesis.

ROS production is increased in *Δβca1ca5* leaves. We assayed the level of ROS in WT and mutant lines (Fig. 7A). Previous studies have shown plant CAs to play a role in preventing the creation of ROS (10, 14). Leaves from the first node of tobacco plants grown in ambient CO_2 were homogenized and the homogenate was suspended in a 5 µM CellROX® Green solution. CellROX® Green undergoes a conformational change when oxidized, resulting in increased fluorescence. *Δβca1ca5* leaves displayed a greatly increased fluorescent signal in comparison to leaves of *Δβca1, Δβca5,* and WT (Fig. 7A). There was also a slight increase in the fluorescent signal in *Δβca5* over *Δβca1* and WT. This fluorescence pattern was also observed in the leaves of node 2 and 3 (data not shown). The increased ROS and resultant cellular damage may play a role in the abnormal leaf phenotype of the double mutant grown at ambient CO_2.

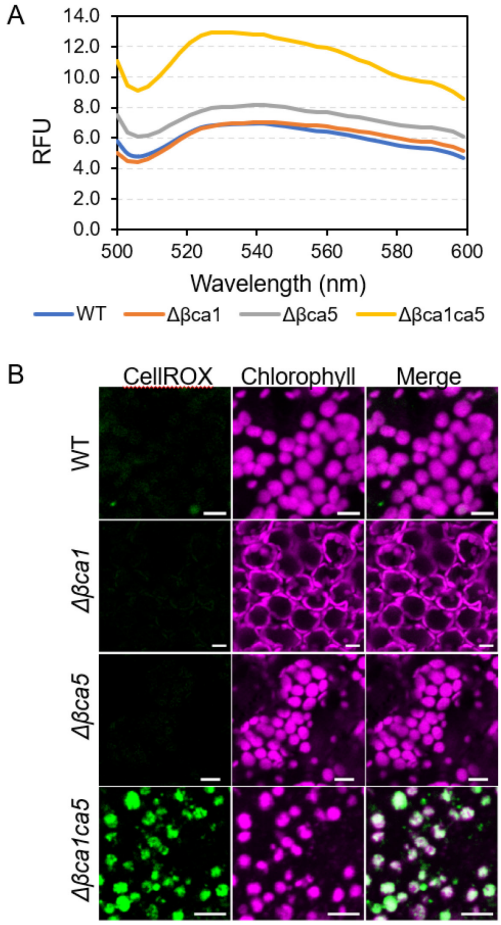

Fig. 7. ROS production. (A) Spectrofluorometer emission spectra of CellROX® Green treated homogenized leaf samples. Signal intensity is in relative fluorescent units (RFU). (B) Confocal

imaging of WT and mutant leaves grown in ambient CO_2 and treated with 5 μM CellROX® Green. Magenta=Chlorophyll autofluorescence, Green=CellROX® Green, Bars=10 μm. Leaves assayed are from the first node of 10-week-old tobacco plants grown for 8 weeks at 9000 ppm CO_2 and 2 weeks at ambient CO_2.

The location of the ROS signals was determined in the mature leaves that had fully developed on plants grown in 9000 ppm CO_2 and were then transferred to ambient CO_2 for 1 week. The ROS signals found in *Δβca1ca5* mesophyll cells appear to be primarily associated with the chloroplast (Fig. 7B), indicating the origins of the increased ROS measured in the *Δβca1ca5* plant *(*Fig. 7A).

Complementation of *Δβca1ca5* mutants. To confirm that the phenotypes observed in *Δβca1ca5* mutants were not a result of off-target mutations caused by the CRISPR/Cas9 system, a series of complementation experiments were performed. For these experiments, *Δβca1ca5* T1 plants lacking the *Cas9* transgene were identified (*SI Appendix*, Fig. S7). Transgene constructs in which the βCA1 CDS and βCA5 CDS were put under the control of the 35S promoter were transformed into *cas9- Δβca1ca5* T1 plants (Fig. 8A). Both *Δβca1ca5*_35S::βCA1 and *Δβca1ca5*_35S::βCA5 complemented the mutant phenotype and produced plants with a gross morphology comparable to WT at ambient CO_2 concentrations (Fig. 8B). This result establishes that the phenotype observed in *Δβca1ca5* tobacco is caused by lack of stromal CA activity and not by an off-target mutation.

The WT phenotype could not be restored to *cas9-Δβca1ca5* plants expressing altered forms of the βCA1 enzyme. We generated a construct in which two of the residues that bind zinc in βCA1 were mutated to adenine (C152A and D152A; shortened hereafter as ΔZn) to make a catalytically inactive form of βCA1 (Fig. 8A). The zinc ion located at the active site cavity of βCAs is essential for the nucleophilicity of the enzyme and thus, its catalytic activity (32). We also generated a construct in which the chloroplast transit peptide (identified as the first 62 amino acids) was removed from βCA1. ΔZn-βCA1 and Δ62-βCA1 were both driven by a 35S overexpression promoter and transformed into *cas9-Δβca1ca5* plants. Neither of these constructs resulted in transgenic plants with normal morphology; instead, the plants showed the characteristic, necrosis-like phenotype at ambient CO_2 (Fig. 8B).

An immunoblot of extracted proteins using an anti-CA1 antibody showed that the mutant and full-length forms of βCA1 were present in the three transgenic lines used in the complementation experiments (Fig. 8C), indicated by a positive band at ~28kDA in leaf homogenate of WT, Δ*βca5*, *Δβca1ca5*_35S::βCA1, *Δβca1ca5*_35S::Δ62-βCA1, and *Δβca1ca5*_35S::ΔZn-βCA1 tobacco plants.

CA activity assays determined that *cas9-Δβca1ca5* plants expressing the cytoplasm-localized βCA1 (Δ62-βCA1) and full length βCA1 or βCA5 had substantially increased CA activity compared to the double mutant (Fig. 8D), signifying that Δ62-βCA1 is still catalytically active. Both *Δβca1ca5*_35S::Δ62-βCA1 and *Δβca1ca5*_35S::ΔZn-βCA1 had heightened ROS levels like *Δβca1ca5*, while *Δβca1ca5*_35S::βCA1 showed a decrease in ROS production (Fig. 8E).

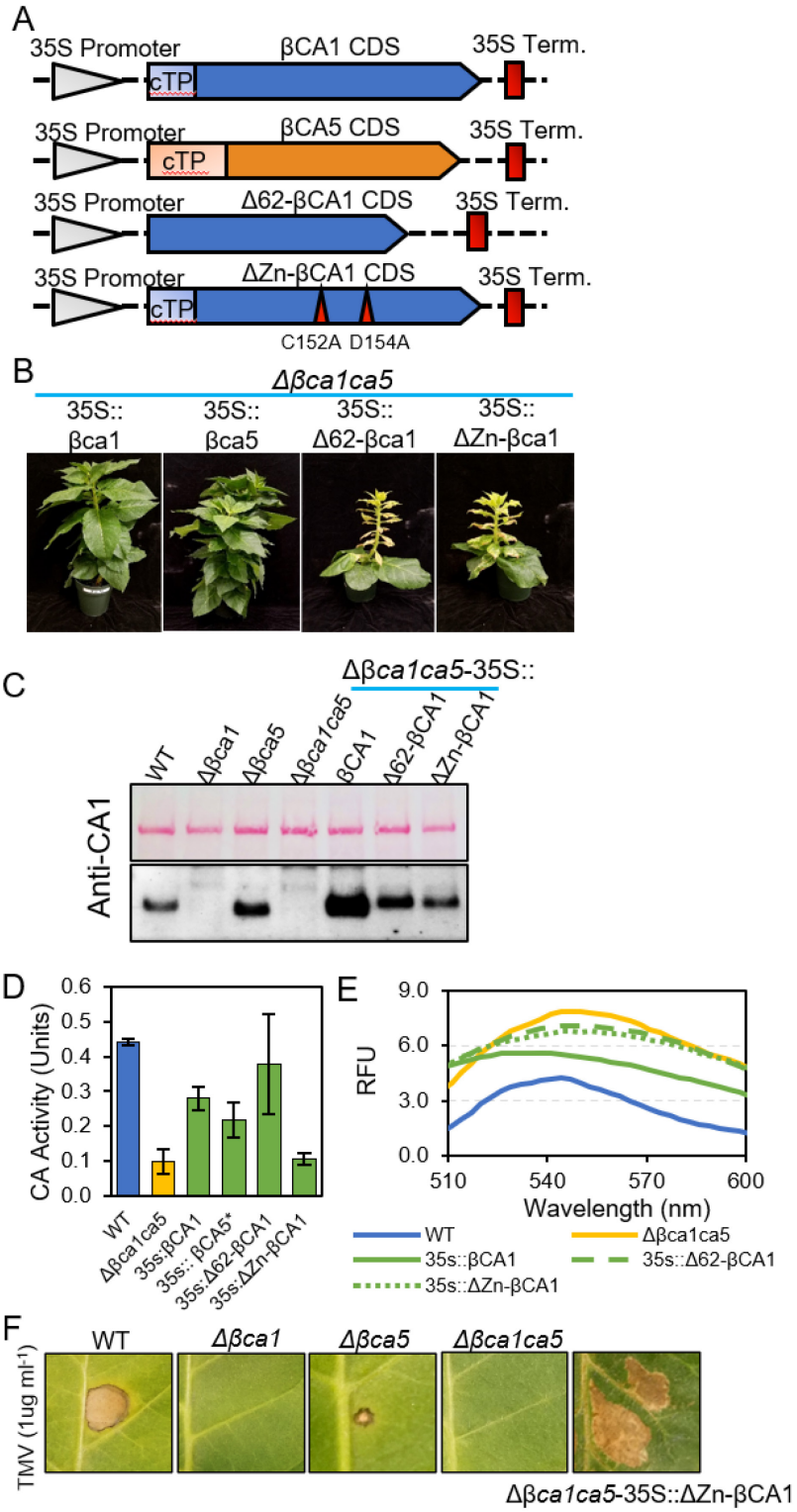

Fig. 8. Complementation of CRISPR-generated *Δβca1ca5* mutant with different forms of CA proteins. (A) Construct diagrams for complementation of *Δβca1ca5* double mutant tobacco. CDS: coding sequencing cTP: chloroplast transit peptide (62 amino acids) TERM: terminator. (B) Morphology of plants grown in high CO_2 then transferred to ambient CO_2 (C) Top: Ponceau

stain showing the RuBisCO large subunit signal. Bottom: Immunoblot of WT, mutant, and complemented lines leaf protein extracts with anti-CA1 antibody. (D) CA activity assay of WT, *Δβca1ca5*, and complemented lines (*CA assay done on the T0 generation). Each assay was performed with 4 samples. Bars=Standard error. (E) Spectrofluorometer emission spectra of CellROX® Green treated homogenized leaf samples. Signal intensity is in relative fluorescent units (RFU). (F) Inoculation of TMV onto fully expanded leaves of WT and transgenic lines.

As previously reported (10), βCA1 is a salicylic acid binding protein that plays a role in the hypersensitive defense response of tobacco. Mature leaves of WT and CA mutant lines, grown at high CO_2, were treated with 5μM of suspended tobacco mosaic virus (TMV) and left in a growth chamber containing ambient CO_2. After three days, WT and *Δβca5* plants displayed the characteristic necrosis at the site of infection, indicating an HR (Fig. 8F). As expected from previous work (10, 11), neither *Δβca1* nor *Δβca1ca5* produced an HR when inoculated with TMV (Fig. 8F). However, *Δβca1ca5*_35S::ΔZn-βCA1 plants display the characteristic programed cell death of an HR, despite their minimal CA activity levels (Fig. 8F). This result suggests that ΔZn-βCA1 is still able to bind to SA and contribute to plant defense even with a mutated catalytic center. These experiments indicate that both the location of βCA1 (in the chloroplast stroma) and its catalytic activity are necessary to complement the *Δβca1ca5* phenotype. In contrast, an inactive βCA1, while not restoring wild-type phenotype, can elicit the HR.

Discussion

Previous experiments that studied single knockouts of βCA1 did not eliminate all CA enzymatic activity from the chloroplast stroma because no lines with both stromal CAs mutated were examined (2, 10, 16). In Arabidopsis, a slow growth and sterility phenotype was observed when βCA5 alone is knocked out (11), suggesting that activity of the other chloroplast CAs in Arabidopsis cannot fully compensate for the absence of βCA5 during development. In contrast, the single mutants in tobacco exhibited normal phenotype. However, eliminating expression of both chloroplast stromal CAs resulted in a striking defect in leaf and floral bud development as well as impaired seed formation. This report presents the first complete disruption of CA activity in the chloroplast stroma and provides insight into its function in C_3 plants.

The role of CAs in C_3 plant photosynthesis has not been established, unlike their role in the C_4 CO_2-concentrating mechanism and photosynthesis (7). The majority of CA activity in C4 plants is present in the cytosol of mesophyll cells (6) and little or no activity is present in bundle sheath cells (33), the site of carbon fixation. C_4 plants with reduced cytosolic CA activity show reduced photosynthetic assimilation especially at decreasing CO_2 levels (34). In C_3 plants, the dominant CA activity is present in stroma and it was postulated that removal of stromal CAs will significantly reduce mesophyll conductance (35). In previous measurements on an antisense-CA1 mutant in tobacco (16), a 99% reduction in CA activity showed no measurable reduction in RuBisCO activity nor CO_2 uptake and the plants exhibited normal development. However, because of the high catalytic rate of CA, even a small amount of CA activity could possibly provide sufficient turnover and result in the lack of any morphological phenotype. To further clarify the role of CA in C3 photosynthesis, we measured CO_2 fixation rates under ambient (21% O_2) and non-photorespiratory conditions (1% O_2) and found no significant difference in assimilation rate at either ambient or saturating CO_2 in the double mutants compared to wild-type (Figs. 5C and 5D, *SI Appendix*, Fig. S5). Likewise, measurements of Φ_{PSII} under ambient CO_2 and O_2 conditions showed no significant differences between wild-type and the Δ*βca1* and

Δβca1ca5 mutants (Fig. 5A). Together these data indicate that stromal CA is not required to provide a sufficient flux of CO_2 from the atmosphere to RuBisCO under either light-saturated steady-state or transient (low light to saturating light) conditions. While we cannot rule out that stromal CA does not affect photosynthetic efficiency in every possible environmental condition, we can conclude that its primary role is not in enhancing carbon fixation.

The similarity between CO_2 fixation rates and Φ_{PSII} measurements between wild-type and the mutants at ambient O_2 also suggests that photorespiratory losses are small under the experimental conditions and are not influenced by the removal of stromal CA activity.

Even though a complete lack of chloroplast CA activity has not been previously reported in plants, absence of CA activity has been reported in bacterial (36-38) and yeast mutants (39, 40). Typically, the CA-less mutants grow poorly at ambient CO_2 levels, but the phenotype can be alleviated by using high CO_2 levels (~5%) or complementing with heterologous CA. The poor growth phenotype in microorganisms is known to be caused by deficiency of bicarbonate, which is an important precursor for carboxylation reactions in several biosynthetic pathways (2, 36, 41). In a fast-growing microbe like *E.coli*, it was calculated that the bicarbonate requirement is 10^3-10^4 fold greater than what could be provided by uncatalyzed hydration of CO_2 (36). In plants, chloroplasts are the primary site for many of these pathways, leading to the logical speculation that CAs are essential to support non-photosynthetic carboxylation pathways, which generally have a high K_m for C_i, at current ambient CO_2 levels (2). It was calculated that even with CAs, such pathways are operating at about 0.5-17% of HCO_3^- saturation, which would make such reactions staggeringly slow in absence of CA and with competition for CO_2 by RuBisCO (2). As the uptake of bicarbonate by chloroplasts is 4 orders of magnitude lower than CO_2 diffusion, as shown by a study with intact chloroplasts (17), and no bicarbonate transporters have been functionally characterized in the chloroplast envelope (42), the pathways requiring bicarbonate in chloroplasts are highly dependent on CA. The mutant phenotype of *Δβca1ca5* leaves grown at ambient CO_2 (Fig. 3A) is lost when the leaves are allowed to fully expand under high (9000 ppm) CO_2 (Fig. 3B) in a manner similar to CA-free unicellular organisms. Note that growth under high CO_2 will, at equilibrium, elevate the stromal CO_2 and bicarbonate levels by about a factor of 20, possibly increasing the rate of formation and concentration of bicarbonate enough to support bicarbonate-dependent carboxylation pathways.

A model for the movement of inorganic carbon from the atmosphere to RuBisCO in C_3 plants is shown in Fig. 9, showing the two theoretical alternatives for moving inorganic C across the chloroplast envelope membranes. Pathway (1) is the direct pathway in which CO_2 crosses the envelope either by passive or facilitated diffusion; aquaporins have been shown to contribute to CO_2 transport into the chloroplast (17). Pathway (2) would utilize passive or active transport of bicarbonate into the chloroplast, with cytoplasmic and stromal CAs catalyzing the interconversion of dissolved CO_2 and bicarbonate. However, there is no evidence for bicarbonate transport into vascular plant chloroplasts (42). As inorganic carbon is not transported in bicarbonate form, removal of CAs should have minimal impact on mesophyll conductance (g_m). We estimated g_m from the assimilation data using the calculator described by Sharkey (43). Although this method gives assimilation-weighted estimates, it is useful in comparing plants in an experiment and we found no significant difference in estimated g_m values of WT and *Δβca1ca5* (Fig. S5C). Within the chloroplast, we propose that CAs provide HCO_3^- for consumption by bicarbonate-dependent carboxylation pathways by maintaining HCO_3^- at equilibrium concentration.

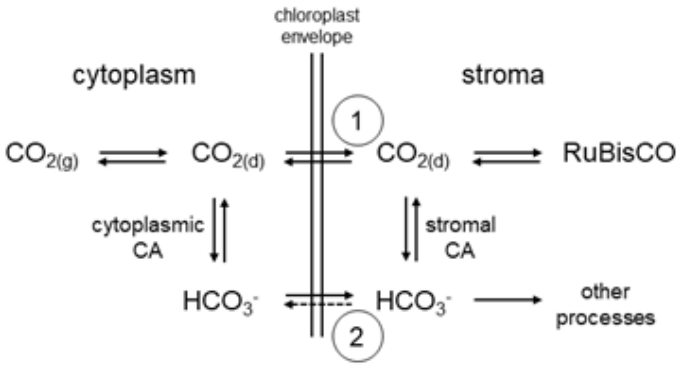

Fig. 9. A simple model for the movement of inorganic C from the atmosphere to RuBisCO in C_3 photosynthesis. $CO_{2\,(g)}$ = gaseous (atmospheric) CO_2, $CO_{2\,(d)}$ = dissolved CO_2. 1: passive or facilitated diffusion of CO_2 across the chloroplast envelope membranes; 2: facilitated diffusion or active transport of bicarbonate across the chloroplast envelope membranes.

In a detailed study of a yeast CA-knockout line (41), the authors attempted to complement specific bicarbonate-dependent pathways by nutritional supplementation. Even though some specific supplementations improved growth, a full nutritional supplementation was not able to completely restore the growth of the CA mutant to the level of the reference strain. The authors suggested that the failure to rescue growth resulted from the inability of the yeast to take up sufficient fatty acids. Similar experiments cannot be performed with plant cells, given the well-known lack of uptake of many types of exogenously supplied nutrients from cell culture. Likewise, a large-scale analysis of metabolite differences between the chloroplast CA-less mutant and wild-type would be predicted to produce a bewildering array of changes due to the large number of pathways affected by limitation of bicarbonate.

Nevertheless, some information about disrupted metabolism following limiting of CA and bicarbonate has been obtained through analysis of fatty acids and lipids. Metabolites whose concentration could be affected by inadequate bicarbonate include malonyl-CoA and its derivatives, which are used in the synthesis of lipids (44). Malonyl-CoA and fatty acid synthesis depend on the enzyme acetyl-CoA Carboxylase (K_m 0.9-2.5 mM), which uses bicarbonate to carboxylate its substrate (2, 45-47). When CA activity in tobacco leaves is suppressed using inhibitors (like ethoxyzolamide) or antisense RNA silencing, the incorporation of acetyl into total lipids is greatly reduced (15). We observed alterations in the FFA profiles of young WT and *Δβca1ca5* leaves (Fig. 4A, S4A). The double mutant had a significant reduction in the amount of 16:0 and 18:0 FFA, both of which arise in the chloroplast before being elongated and further modified in other organelles. Previously it had been observed that suppressing CA activity resulted in improper incorporation of acetyl into lipids of developing cotton (*Gossypium hirsutum)* embryos and an increase in seedling lethality in Arabidopsis (15, 48). We detected morphological defects and a similar drop in the germination of seeds in the *Δβca1ca5* double mutant (Fig. 4). Importantly, Hoang and Chapman (15) demonstrated that inhibition of plastid CA activity resulted in the reduced incorporation of acetyl into lipids in antisense CA tobacco lines.

Further evidence for the need of CAs for biosynthesis comes from considering the disruption of the sink-to-source transition in the double mutant. Normal leaf development involves a metabolic transition of the leaf from sink to source; this transition does not occur uniformly in the leaf but

begins at the tip and ends at the base of the leaf (49). In parallel with this developmental pattern, we observe that when developing *Δβca1ca5* leaves are moved from high CO_2 to ambient CO_2, areas of the leaf closest to the tip do not display the mutant phenotype, while areas closer to the leaf base develop the characteristic lesions (Fig. 3C, blue arrow and Fig. 3D). Interestingly, leaves which develop completely at ambient CO_2 show a different pattern where necrosis begins at the tip and spreads to the base (Fig. 3G). Thus, the part of an expanding leaf that has completed the sink-to-source transition (closer to the tip) at the time it is transferred from high to ambient CO_2 is less likely to exhibit the mutant phenotype than the base of the leaf which has not completed this transition.

We observed a rise in chloroplast ROS, which may be a contributor to the double mutant's leaf phenotype when grown at ambient CO_2. The increase in ROS in the double mutant is consistent with our observation of a significant decrease in F_v/F_m and in the yield of non-photochemical quenching (Φ_{NPQ}) in the *Δβca1ca5* mutant (Fig. 5B). Under most conditions, the yields of photochemical and non-photochemical quenching are complementary – for every incremental change in Φ_{PSII} there is a complementary change in Φ_{NPQ} (50). A breakdown in this complementarity, as seen in the double mutant, necessarily leads to increased production of ROS. Although newly budded leaves of the *Δβca1ca5* double mutant in ambient CO_2 appear like WT in gross morphology, the leaf does exhibit higher ROS localized to the chloroplast (Figs. 7A and 7B), which may set the pathway to necrosis in motion.

βCA1 has been shown to bind the plant hormone salicylic acid (SA) (10) and is involved in the perception of SA levels in plant (11). When Slaymaker et al (10) silenced βCA1 in *Nicotiana tabacum*, they observed an absence of an HR when the leaves were transiently transformed by Agrobacterium expressing *Pto* and *avrPto*. We also observed a lack of HR in *Δβca1* and *Δβca1ca5* plants (Fig. 8F). Even though *Δβca1ca5* plants expressing a zinc-binding site mutated βCA1 (ΔZn-βCA1) were unable to complement the developmental mutant phenotype at ambient CO_2 concentrations (Fig. 8B), expression of the mutant protein was able to complement HR defect (Fig. 8C, 8F). This finding implies that the protein's ability to bind SA has not been compromised by the zinc-binding site mutations at its catalytic core. These plants can induce programmed cell death in response to a pathogen but still demonstrate leaf necrosis at ambient CO_2, which indicates that the ΔZn-βCA1 has no CA activity. Thus, chloroplast CA activity can be removed from a plant without removing its ability to respond to viruses through an HR.

Inorganic carbon concentrations at ambient conditions are not expected to play a significant role in pH buffering in the chloroplast (2). While the pH measurements we performed were not quantitative, they do provide insight into the relative sizes of the bicarbonate and CO_2 pools when the absence of stromal CA prevents rapid equilibration of the two pools. The *Δβca1ca5* mutant showed an increased ratio between the 405nm and 488nm emission signals, indicating a more basic stroma compared to WT and the single mutants *Δβca1* and Δβca5 (Fig. 5A). Our observation that photosynthesis is unaffected in the *Δβca1ca5* mutant suggests that any disruption of stromal pH in the mutant is not sufficient to alter the rate of photosynthesis.

In summary, CRISPR-generated knockout lines in tobacco demonstrate that CA activity in the chloroplast stroma is required for normal plant and seed development at ambient CO_2 concentrations, but not for supplying CO_2 for photosynthesis. Removing CA activity from the chloroplast stroma results in large necrotic lesions in developing leaf tissue and reduced germination of seeds following growth in ambient CO_2. Both mutant phenotypes can be prevented by growing *Δβca1ca5* plants in high CO_2 concentrations of 9000 ppm. These

phenotypes and their relief in high CO_2 point to underlying defects in metabolism, which is starvation of bicarbonate-dependent enzymes in absence of CA activity. We show that such a defect is also accompanied by elevated levels of ROS which may play a role in the manifestation of necrotic lesions.

Typically, algal and bacterial systems that rely on HCO_3^- transporter-based CO_2-concentrating mechanisms either have highly regulated CA activity in stroma or no CAs in the cytoplasm, respectively. Schemes to produce a functional carboxysome or artificial pyrenoid in chloroplasts propose the incorporation of bicarbonate transporters on the chloroplast envelope membrane along with the removal of stromal CAs (18, 51, 52). We provide evidence that the HR could be maintained in plants engineered to lack CA, provided that a catalytically inactive CA is incorporated. CA catalytic activity is not necessary for photosynthesis but to provide bicarbonate for biosynthetic pathways, which would be rendered functional by a bicarbonate transporter. Thus, our work supports the feasibility of an important step in the engineering of a CO_2-concentrating mechanism into a C_3 plant.

Materials and Methods

Transformation constructs to produce YFP fusion for CA localization or complement mutants. The TargetP online prediction program (53) was used to identify candidate CA proteins that might be located in the chloroplast. Production of cDNA, cloning into vectors with YFP at the C-terminus and transient expression is described in *SI Appendix, Supplementary Materials and Methods*, where details of cloning of complementation constructs can also be found.

Design and assembly of CRISPR/Cas9 constructs. The CCTop online program was used to identify and select CRISPR/Cas9 sgRNA target sites in the βca1 and βca5 genes (54). Further details can be found in *SI Appendix, Supplementary Materials and Methods*

Agrobacterium-mediated transformation of tobacco. Transformation of tobacco generally followed the protocol described in Sparkes et al. (2006). Further information can be found in *SI Appendix, Supplementary Materials and Methods.*

Production of anti-CA1 polyclonal antisera. The peptide SLPADGSESTAFIEC was synthesized and conjugated to keyhole limpet hemocyanin and used to immunize two rabbits by Pocono Rabbit Farm and Laboratory, Inc (Canadensis, PA). One of the protein A-purified antisera reacted with proteins from WT on immunoblot at the expected molecular mass for CA1 and did not detect a protein in *Δβca1* or *Δβca1ca5* tissue but does detect CA1 in *Δβca5* plants, as expected.

Growth chamber conditions. Plants were grown under 100 μmol/m^2/s photosynthetically active radiation (PAR) with a 16-hour photoperiod in ambient and high (9000 ppm) CO_2 growth chambers. Growth room temperatures were maintained at an average of 22ºC with 50% relative humidity during daylight conditions for the ambient CO_2 chamber and 64% relative humidity for the high CO_2 chamber. Plants were germinated and grown in pots containing LM-111 All Purpose Mix (Lambert), watered daily in the morning by hand, and kept in free-draining flats.

CA activity assay. The CA activity assay was carried out as previously described (11) with slight modifications. Further information can be found in *SI Appendix, Supplementary Materials and Methods.*

ROS Assay. Tissue was labeled with the fluorescent dye CellROX® Green (Thermofisher Scientific Cat. No. C10444) and examined in a spectrofluorometer and a confocal microscope. Further information can be found in *SI Appendix, Supplementary Materials and Methods.*

pH measurements with pHlourin2. The plasmid pME-pHluorin2 was a gift from David Raible (Addgene plasmid # 73794; http://n2t.net/addgene:73794 ; RRID:Addgene_73794) (31, 55). The pHlourin2 protein sequence was altered with the addition of the chloroplast transit peptide from the Arabidopsis RecA DNA recombination family protein (accession NM_001084375.1) to its N-terminus.

Chlorophyll fluorescence and gas exchange measurements. Chlorophyll fluorescence was measured on intact plants using WALZ Imaging PAM M-series chlorophyll fluorometer (Heinz Walz GmbH, Effeltrich, Germany). The LI-6800 Portable Photosynthesis System© (Li-Cor Biosciences) was used for assay of net CO_2 fixation and internal (leaf) CO_2 concentration.

Assay of leaf free fatty acids. Young leaves from the first 3 nodes of WT tobacco and the *Δβca1ca5* mutant were ground into powder in liquid nitrogen, extracted, and assayed by mass spectrometry as described in *SI Appendix, Supplementary Materials and Methods.*

TMV Inoculation
Inoculation with TMV was performed similarly to the method of Guo et al (56) as described in *SI Appendix, Supplementary Materials and Methods.*

Data Availability
All study data are included in the article and supporting information or have been contributed to Genbank.

ACKNOWLEDGMENTS. The authors would like to thank Dr. Joyce Van Eck and Dr. Daniel Klessig of the Boyce Thompson Institute for the plasmids containing Cas9+sgRNA and for use of their growth facilities for the TMV inoculation, respectively. We would also like to thank Dr. M. Elena Diaz Rubio (Cornell Metabolomics Facility) for performing mass spectrometry for fatty acid composition. K.N.E. participated in the Cornell Dept. of Molecular Biology and Genetics NSF REU program (DBI-1659534). Acquisition of equipment for the work was partially supported through a Cornell University Institute of Biotechnology's Center for Advanced Technology (CAT) grant, funded through New York State Division of Science, Technology, and Innovation (NYSTAR) and NYS contract C150124 (grant number NIH S10RR025502 for data collected on the Zeiss LSM 710 Confocal). The major funding was from Bilateral NSF-BIO/BBSRC 1642386 to M.R.H

References

1. J. M. Berg, J. L. Tymoczko, L. Stryer, L. Stryer, *Biochemistry* (W.H. Freeman, New York, ed. 5th, 2002).
2. R. J. DiMario, M. C. Machingura, G. L. Waldrop, J. V. Moroney, The many types of carbonic anhydrases in photosynthetic organisms. *Plant Sci* **268**, 11-17 (2018).
3. A. Tiwari, P. Kumar, S. Singh, S. A. Ansar, Carbonic anhydrase in relation to higher plants. *Photosynthetica* **43**, 1-11 (2005).
4. J. Floryszak-Wieczorek, M. Arasimowicz-Jelonek, The multifunctional face of plant carbonic anhydrase. *Plant Phys Biochem : PPB* **112**, 362-368 (2017).
5. M. D. Hatch, J. N. Burnell, Carbonic anhydrase activity in leaves and its role in the first step of C_4 photosynthesis. *Plant Physiol* **93**, 825-828 (1990).
6. M. R. Badger, G. D. Price, The role of carbonic anhydrase in photosynthesis. *Ann Rev Plant Phys Plant MolBiol* **45**, 369-392 (1994).
7. M. Momayyezi, A. D. McKown, S. C. S. Bell, R. D. Guy, Emerging roles for carbonic anhydrase in mesophyll conductance and photosynthesis. *Plant J* **101**, 831-844 (2020).
8. N. Fabre, I. M. Reiter, N. Becuwe-Linka, B. Genty, D. Rumeau, Characterization and expression analysis of genes encoding alpha and beta carbonic anhydrases in Arabidopsis. *Plant Cell Environ* **30**, 617-629 (2007).
9. R. J. DiMario *et al.*, The cytoplasmic carbonic anhydrases betaCA2 and betaCA4 are required for optimal plant growth at low CO_2. *Plant Physiol* **171**, 280-293 (2016).
10. D. H. Slaymaker *et al.*, The tobacco salicylic acid-binding protein 3 (SABP3) is the chloroplast carbonic anhydrase, which exhibits antioxidant activity and plays a role in the hypersensitive defense response. *Proc Natl Acad Sci U S A* **99**, 11640-11645 (2002).
11. L. Medina-Puche *et al.*, beta-carbonic anhydrases play a role in salicylic acid perception in Arabidopsis. *PloS one* **12**, e0181820 (2017).
12. H. Hu *et al.*, Distinct cellular locations of carbonic anhydrases mediate carbon dioxide control of stomatal movements. *Plant Physiol* **169**, 1168-1178 (2015).
13. H. Hu *et al.*, Carbonic anhydrases are upstream regulators of CO_2-controlled stomatal movements in guard cells. *Nature Cell Biol* **12**, 87-93; sup pp 81-18 (2010).
14. J. Dabrowska-Bronk *et al.*, beta-carbonic anhydrases and carbonic ions uptake positively influence Arabidopsis photosynthesis, oxidative stress tolerance and growth in light dependent manner. *J Plant Physiol* **203**, 44-54 (2016).
15. C. V. Hoang, K. D. Chapman, Biochemical and molecular inhibition of plastidial carbonic anhydrase reduces the incorporation of acetate into lipids in cotton embryos and tobacco cell suspensions and leaves. *Plant Physiol* **128**, 1417-1427 (2002).
16. G. D. Price *et al.*, Specific reduction of chloroplast carbonic anhydrase activity by antisense RNA in transgenic tobacco plants has a minor effect on photosynthetic CO_2 assimilation. *Planta* **193**, 331-340 (1994).
17. D. Tolleter, V. Chochois, R. Poire, G. D. Price, M. R. Badger, Measuring CO_2 and HCO_3^- permeabilities of isolated chloroplasts using a MIMS-18O approach. *J Exp Bot* **68**, 3915-3924 (2017).
18. M. R. Hanson, M. T. Lin, A. E. Carmo-Silva, M. A. Parry, Towards engineering carboxysomes into C3 plants. *Plant J* **87**, 38-50 (2016).
19. N. Atkinson *et al.*, Introducing an algal carbon-concentrating mechanism into higher plants: location and incorporation of key components. *Plant Biotech J* **14**, 1302-1315 (2016).

20. M. R. Badger, G. D. Price, CO_2 concentrating mechanisms in cyanobacteria: molecular components, their diversity and evolution. *J Exp Bot* **54**, 609-622 (2003).
21. G. D. Price, M. R. Badger, Expression of human carbonic anhydrase in the cyanobacterium *Synechococcus* PCC7942 creates a high CO_2-requiring phenotype : Evidence for a Central Role for Carboxysomes in the CO_2 Concentrating Mechanism. *Plant Physiol* **91**, 505-513 (1989).
22. J. M. McGrath, S. P. Long, Can the cyanobacterial carbon-concentrating mechanism increase photosynthesis in crop species? A theoretical analysis. *Plant Physiol* **164**, 2247-2261 (2014).
23. A. Villarejo *et al.*, Evidence for a protein transported through the secretory pathway en route to the higher plant chloroplast. *Nature Cell Biology* **7**, 1224-1231 (2005).
24. I. M. Roberts *et al.*, Dynamic changes in the frequency and architecture of plasmodesmata during the sink-source transition in tobacco leaves. *Protoplasma* **218**, 31-44 (2001).
25. J. Melkonian, T. G. Owens, D. W. Wolfe, Gas exchange and co-regulation of photochemical and nonphotochemical quenching in bean during chilling at ambient and elevated carbon dioxide. *Photosynth Res* **79**, 71-82 (2004).
26. H. Bauwe, M. Hagemann, A. R. Fernie, Photorespiration: players, partners and origin. *Trends Plant Sci* **15**, 330-336 (2010).
27. A. Gerbaud, M. Andre, Effect of CO_2, O_2, and light on photosynthesis and photorespiration in wheat. *Plant Physiol* **66**, 1032-1036 (1980).
28. X. Ren, S. Lindskog, Buffer dependence of CO_2 hydration catalyzed by human carbonic anhydrase I. *Biochim Biophys Acta* **1120**, 81-86 (1992).
29. B. S. Jacobson, F. Fong, R. L. Heath, Carbonic anhydrase of spinach: studies on Its location, inhibition, and physiological function. *Plant Physiology* **55**, 468-474 (1975).
30. A. T. Jagendorf, E. Uribe, ATP formation caused by acid-base transition of spinach chloroplasts. *Proc Natl Acad Sci USA* **55**, 170-177 (1966).
31. M. J. Mahon, pHluorin2: an enhanced, ratiometric, pH-sensitive green florescent protein. *Adv Biosci Biotechnol* **2**, 132-137 (2011).
32. Claudiu T. Supuran, Structure and function of carbonic anhydrases. *Biochem J* **473**, 2023-2032 (2016).
33. J. N. Burnell, M. D. Hatch, Low bundle sheath carbonic anhydrase is apparently essential for effective c(4) pathway operation. *Plant Physiol* **86**, 1252-1256 (1988).
34. S. Von Caemmerer *et al.*, Carbonic anhydrase and C_4 photosynthesis: a transgenic analysis. *Plant Cell Environ.* **27**, 697-703 (2004).
35. D. Tholen, X. G. Zhu, The mechanistic basis of internal conductance: a theoretical analysis of mesophyll cell photosynthesis and CO2 diffusion. *Plant Physiol* **156**, 90-105 (2011).
36. C. Merlin, M. Masters, S. McAteer, A. Coulson, Why is carbonic anhydrase essential to *Escherichia coli*? *J Bacteriol* **185**, 6415-6424 (2003).
37. P. Burghout *et al.*, Carbonic anhydrase is essential for *Streptococcus pneumoniae* growth in environmental ambient air. *J Bacteriol* **192**, 4054-4062 (2010).
38. J. J. Desmarais *et al.*, DABs are inorganic carbon pumps found throughout prokaryotic phyla. *Nat Microbiol* **4**, 2204-2215 (2019).

39. R. Gotz, A. Gnann, F. K. Zimmermann, Deletion of the carbonic anhydrase-like gene NCE103 of the yeast *Saccharomyces cerevisiae* causes an oxygen-sensitive growth defect. *Yeast* **15**, 855-864 (1999).
40. T. Klengel *et al.*, Fungal adenylyl cyclase integrates CO_2 sensing with cAMP signaling and virulence. *Curr Biol* **15**, 2021-2026 (2005).
41. J. Aguilera, J. P. Van Dijken, J. H. De Winde, J. T. Pronk, Carbonic anhydrase (Nce103p): an essential biosynthetic enzyme for growth of *Saccharomyces cerevisiae* at atmospheric carbon dioxide pressure. *Biochem J* **391**, 311-316 (2005).
42. C. Poschenrieder *et al.*, Transport and use of bicarbonate in plants: current knowledge and challenges ahead. *Int J Mol Sci* **19** (2018).
43. T. D. Sharkey, What gas exchange data can tell us about photosynthesis. *Plant, Cell & Environment* **39**, 1161-1163 (2016).
44. V. Gueguen, D. Macherel, M. Jaquinod, R. Douce, J. Bourguignon, Fatty acid and lipoic acid biosynthesis in higher plant mitochondria. *J Biol Chem* **275**, 5016-5025 (2000).
45. B. J. Nikolau, J. C. Hawke, Purification and characterization of maize leaf acetyl-coenzyme a carboxylase. *Archiv Biochem Biophys* **228**, 86-96 (1984).
46. C. Alban, P. Baldet, R. Douce, Localization and characterization of two structurally different forms of acetyl-CoA carboxylase in young pea leaves, of which one is sensitive to aryloxyphenoxypropionate herbicides. *Biochem J* **300**, 557-565 (1994).
47. D. Herbert *et al.*, Kinetic studies on two isoforms of acetyl-CoA carboxylase from maize leaves. *Biochem J* **318**, 997-1006 (1996).
48. F. J. Ferreira, C. Guo, J. R. Coleman, Reduction of plastid-localized carbonic anhydrase activity results in reduced Arabidopsis seedling survivorship. *Plant Physiol* **147**, 585-594 (2008).
49. R. Turgeon, The sink-source transition in leaves. *Ann Rev Plant Physiol Plant Mol Biology* **40**, 119-138 (1989).
50. J. Melkonian, D. W. Wolfe, T. G. Owens, Effects of elevated carbon dioxide on gas exchange and photochemical and nonphotochemical quenching at low temperature in tobacco plants varying in RuBisCO activity. *Photosynth Res* **83**, 63-74 (2005).
51. B. M. Long *et al.*, Carboxysome encapsulation of the CO_2-fixing enzyme RuBisCO in tobacco chloroplasts. *Nat Commun* **9**, 3570 (2018).
52. R. E. Sharwood, A step forward to building an algal pyrenoid in higher plants. *New Phytol* **214**, 496-499 (2017).
53. O. Emanuelsson, S. Brunak, G. von Heijne, H. Nielsen, Locating proteins in the cell using TargetP, SignalP and related tools. *Nat Protoc* **2**, 953-971 (2007).
54. M. Stemmer, T. Thumberger, M. Del Sol Keyer, J. Wittbrodt, J. L. Mateo, CCTop: an intuitive, flexible and reliable CRISPR/Cas9 target prediction tool. *PloS one* **10**, e0124633 (2015).
55. T. M. Stawicki *et al.*, The zebrafish merovingian mutant reveals a role for pH regulation in hair cell toxicity and function. *Dis Model Mech* **7**, 847-856 (2014).
56. A. L. Guo, G. Salih, D. F. Klessig, Activation of a diverse set of genes during the tobacco resistance response to TMV is independent of salicylic acid; induction of a subset is also ethylene independent. *Plant J* **21**, 409-418 (2000).

Supplementary Text

Supplementary Materials and Methods

Production of CA-YFP fusion constructs and transient expression. RNA was isolated from mature *N. tabacum* plants and reverse transcription was performed using universal primers to obtain cDNA. βCA1, βCA5, and αCA1 cDNAs were amplified and PCR products were inserted into the pCR8/GW/TOPO® vector by TA cloning. The CA sequences were then fused to YFP at their C-termini by insertion into the pEXSG-eYFP vector via an LR clonase II reaction. Electrocompetent *Agrobacterium tumefaciens* (GV3101::RK) cells were transformed with the pEXSG-CA-eYFP vectors and then used to transiently transform young *N. tabacum* plant leaves (1). The plants were imaged on a confocal microscope after 48 hours. The βCA5 cDNA sequence has been deposited into GenBank with the accession number BankIt2241503 beta_carbonic_anhydrase_5 MN153507.

Generation of complemented plants. Full-length βCA1 and βCA5 coding sequences were generated from the plasmids used to produce YFP fusions. Primers (which added SpeI and AscI restriction enzyme sites) were used to re-add the stop codon to the full-length CDS and additional primers were used to generate Δ62-βCA1. The plasmid pK7WGF2::hCas9 (AddGene: 46965) was used as the backbone and a restriction digestion was performed to replace the 35S-driven hCas9 gene with βCA1, βCA5, and Δ62-βCA1. The zinc-binding mutant was generated using NEB's Q5® Site-Directed Mutagenesis Kit and primers designed by the NEBaseChanger™ tool.

Transformation of tobacco generally followed the protocol described in Sparkes et al. (2006). Briefly, leaves from two-month-old tobacco Samsun NN plants were injected with a liquid culture of GV3101 (*Agrobacterium tumefaciens*) cells measuring an OD_{600} of 0.5. Inoculated plants were grown in a long day (16 hr) chambers for two days. The inoculated leaves were sterilized in 75% ethanol for 10 seconds and 20% bleach solution for 20 minutes. MS104 (regular MS media with 6-benzylaminopurine [Sigma B3274] and α-naphthalene acetic acid [Sigma N1641]) media containing 3% sucrose and 75 µg/mL kanamycin was used for selection and generation of transformed shoots.

To identify *Δβca1ca5* $Cas9^-$ plants following Agrobacterium-mediated transformation, plants were genotyped using primers that flanked the insert on the plasmid sequence (Table S1).

CRISPR/Cas9 mutagenesis. Target sites were chosen to be <150 bp apart to create large deletions that could easily be genotyped by PCR (Fig. S2). Constructs containing the Cas9 enzyme gene and sgRNA sequences were assembled using the Golden Gate cloning method (2). For the single knockout lines, the two sgRNA sequences for either *βca1* or *βca5* were put under the control of an Arabidopsis ubiquitin 6 promoter (from pICH86966) and inserted into pICH47751 and pICH47761 plasmids. The sgRNA constructs along with the Cas9 (pICH47742 2x35S-5'UTR-hCas9), the kanamycin selectable marker (pICSL11024 NOSp-NPTII-OCST), and the linker (pICH41780)

constructs were then assembled into the final, level-2 construct pAGM4723 (3, 4) and transformed into plant tissue as described above. For the double knockout lines, pICH47781 and pICH47791 were used for the βca5 sgRNA targets. Guide RNAs and primers are shown in Table S1.

Genotyping and sequencing transformed lines. Rooted transformed plants were used in genotyping. With primers specific for Cas9, the MyTaq™ Plant-PCR kit (BIO-25055) was used to identify plants containing the T-DNA insertion and to determine whether there was a change in the PCR product derived from the CA genes. Genomic DNA was isolated from transgenic plants with cetyltrimethylammonium bromide (CTAB). Phusion DNA polymerase was used to amplify the mutated CA genes. Because of the possibility that there could be a variety of mutations present in PCR products of approximately the same size, a colony library was created by cloning the PCR products into the pCR®2.1 TOPO vector, transforming *E. coli*, and plating. Colonies were cultured, and the individual plasmids were isolated and sequenced.

CA activity assay. The CA activity assay was carried out as previously described (5) with slight modifications. Small leaf samples from mature plants were homogenized in 200 mM Tris-HCl, pH 8.3, 1 mM EDTA, 20 mM $MgCl_2$, 50 mM NaCl, and 100 mM Na_2SO_4 in a 3:1 ratio (volume:weight). 100µL of homogenate was mixed with 200 µL of 20 mM Tris-HCl, pH 8.3 with bromothymol blue. The reaction was started by adding 700 µL of cold carbonated ddH_2O. Water was carbonated in a SodaStream® system (item model number 1012111015) and incubated on ice for 30 minutes before use in assays. The time it took for the mixture to drop from pH 8.3 to 5.5 (indicated by the dye turning from blue to yellow) was recorded, with the same procedure being followed in a control tube lacking tissue. The units of enzyme activity were calculated as: *1 unit = (Tb/Ts-1)/ (Ts*P)*, where *Tb* and *Ts* represent the time (in seconds) it took for the pH to drop from 8.3 to 5.5 in the control and plant homogenate reactions, respectively (6), and represent the protein concentration in milligrams. Each sample and control was used in replicates of four and reactions took place on ice.

ROS Assay. Emergent leaves from the first node of 10-week-old tobacco plants grown for 8 weeks at 9000ppm CO_2 and 2 weeks at ambient CO_2 were used to measure the presence of ROS using the fluorescent dye CellROX® Green (Thermofisher Scientific Cat. No. C10444). The original protocol was adapted for use on plant tissues. Briefly, whole leaf samples were frozen in liquid nitrogen, ground into a powder, and suspended in 5µM of CellROX® Green in homogenization buffer (200 mM Tris-HCl, pH8.3, 1 mM EDTA, 20 mM $MgCl_2$, 50 mM NaCl, 100 mM Na_2SO_4). After being incubated at room temperature for 30 minutes, samples were then measured on a PTI spectrofluorometer using an excitation wavelength of 480 nm. For confocal imaging CellROX® Green was diluted into 5 µM in ddH_2O and injected into expanding leaves at the third node using a needleless syringe. Treated plants were incubated for 30 minutes at room temperature. Leaf samples were cut out and imaged on a Zeiss LSM710 inverted confocal microscope using the 488 nm laser line.

pH measurements with pHlourin2. The plasmids pBI121-gus +3xFLAG-Strep+GWb and pME-RecAcTP-pHluorin2 were used in a Gateway cloning reaction to produce pBI121-RecAcTP-pHluorin2. Primers are shown in Table S1. WT and transgenic tobacco lines were transiently transformed with Agrobacterium similarly to the YFP fusion localization methods described above. The plants grew in ambient CO_2 (16-hour days, 61 µM light) and were imaged on a confocal microscope 38- and 72-hours post-transformation. The samples were excited under light conditions with 633 nm (2.0%), 405 nm (3.0%), and 488 nm (17%) wavelength lasers with a detectable emission range between 500 nm and 530 nm (for the 405 and 488 laser lines). Emission signal intensity was measured in chloroplasts with the ratio being calculated by dividing the average signal intensity from the 405 nm laser by the 488 nm laser.

Assay of free fatty acids. Young leaves from the first 3 nodes of WT tobacco and the *Δβca1ca5* mutant were ground in a liquid-nitrogen treated mortar and pestle to create 3 replicates of powder with 250 mg fresh weight. 100 mg of sample were placed in a high force Eppendorf tube, and after adding 300 µL of ultrapure water, the mixture was vortexed for 30 s. 187 µL of DCM/MeOH (2:1, by volume) was added, vortexed, and the samples were left on ice 30 min. After 30 min, 400 µL of dichloromethane (DCM) were added and vortexed and then another 400 µL of ultrapure water was added and vortexed again. Finally, the extracts were centrifuged at 13,000 rpm for 15 minutes at 4 °C. The bottom organic layer was collected into glass tubes and dried down by speed vacuum. The residues were reconstituted in 150 µL of IPA/ACN/H2O (65/30/5) that contains heptadecanoic acid as internal standard for normalization.

Samples were sent to the Metabolomics Facility at Cornell University's Biotechnology Resource Center. Analysis was conducted on a Thermo Scientific™ Vanquish™ Horizon UHPLC / Thermo Scientific™ Q Exactive™ HF hybrid quadrupole-Orbitrap mass spectrometer.

Chlorophyll fluorescence measurements. Chlorophyll fluorescence was measured on intact plants using a WALZ Imaging PAM M-series chlorophyll fluorometer (Heinz Walz GmbH, Effeltrich, Germany). Samples were positioned such that the leaf surfaces were between 18 and 19 cm from the LED array. All samples were adapted to a light intensity of 7 µmoles photons m^{-2} s^{-1} for a minimum of 30 minutes before measurement. Samples were then imaged using the non-actinic measuring light (470 nm, frequency = 1Hz) and three to five 1-cm diameter areas of interest (AOI) were defined on sections of each leaf that did not include major veins. Leaves selected for measurement were approximately the same developmental state among treatments. After an initial measurement of the steady-state fluorescence at 7 µmoles photons m^{-2} s^{-1} actinic intensity, the plants were exposed to continuous 790 µmoles photons m^{-2} s^{-1} light from the LED array. Starting at 10 seconds after the increase in actinic intensity, Φ_{PSII} was measured at one-minute intervals using a saturating pulse intensity of 1790 µmoles photons m^{-2} s^{-1} until a steady state was reached (typically 8-12 minutes). Reported Φ_{PSII} values were averaged over 3-5 AOIs per leaf, 2-3 leaves per plant and 2-4 plants per genotype.

Gas exchange measurements. Net CO_2 fixation (A) and internal (leaf) CO_2 concentration (C_i) were measured at saturating light and 1% O_2 (to eliminate photorespiration) on 8-week-old WT and mutant tobacco plants grown in 9000 ppm CO_2 with a photoperiod of 16 hours and illumination of 61 µmol m^{-2} s^{-1} photosynthetically active radiation. The LI-6800 Portable Photosynthesis System© (Li-Cor Biosciences) was used for assay with following settings: Light intensity = 800 µmol m^{-2} s^{-1}, Gas flow = 500 µmol s^{-1} with CO_2 concentration ranging from 0-1600 ppm, Vapor-pressure deficit (VPD leaf) = 1 kPa, Temp = 25 C. An external compressed gas tank of 1% oxygen and 99% nitrogen was connected to the Li-COR instrument to supply gas for low O_2 A/C_i measurements. Measurements were made on a single leaf from 4 plants for each genotype. For 1% O_2, data are from one leaf from four different plants in each genotype, while ambient O_2 data utilized 3 plants of each genotype. Plants were similarly grown and measured for ambient level A/Ci measurements with minor adjustments to the settings: Light intensity = 600 µmol m^{-2} s^{-1}, Gas flow = 400 µmol s^{-1} with CO_2 conc. ranging from 25-2000 ppm, RH = 65%, Temp = 25 C. The A/Ci curve data was used to estimate mesophyll conductance (g_m) using the calculator described by Sharkey (7). The data range was categorized as Rubisco limited (at <250 ppm C_i), RuBP limited (at 250 ppm C_i – saturating C_i) and TPU limited (at saturating C_i) according to method author recommendations. Default settings of constants for tobacco were used. This calculator provides an assimilation-weighted estimate.

TMV Inoculation. WT and mutant tobacco plants were grown at 9000 ppm CO_2 for 8 weeks before being transferred to ambient CO_2. The genetic background of all lines is *Nicotiana tabacum* L. cv. Samsun-NN, which is resistant to TMV as a result of the *N* gene product interfering with the TMV replicase (8, 9). Two fully expanded leaves were chosen from each plant for inoculation (n=10). TMV was diluted to 1 µg mL^{-1} in 25 mM sodium phosphate buffer pH 7.2. Carborundum was sprinkled on the leaves to induce wounding and allow virus entry. A cheesecloth was rinsed in the phosphate solution and then soaked in the diluted TMV/Sodium phosphate solution. Cheesecloth was rubbed on selected leaves and plants were incubated for 45 minutes before being washed with clean ddH_2O. Plants were imaged 6 days post-inoculation.

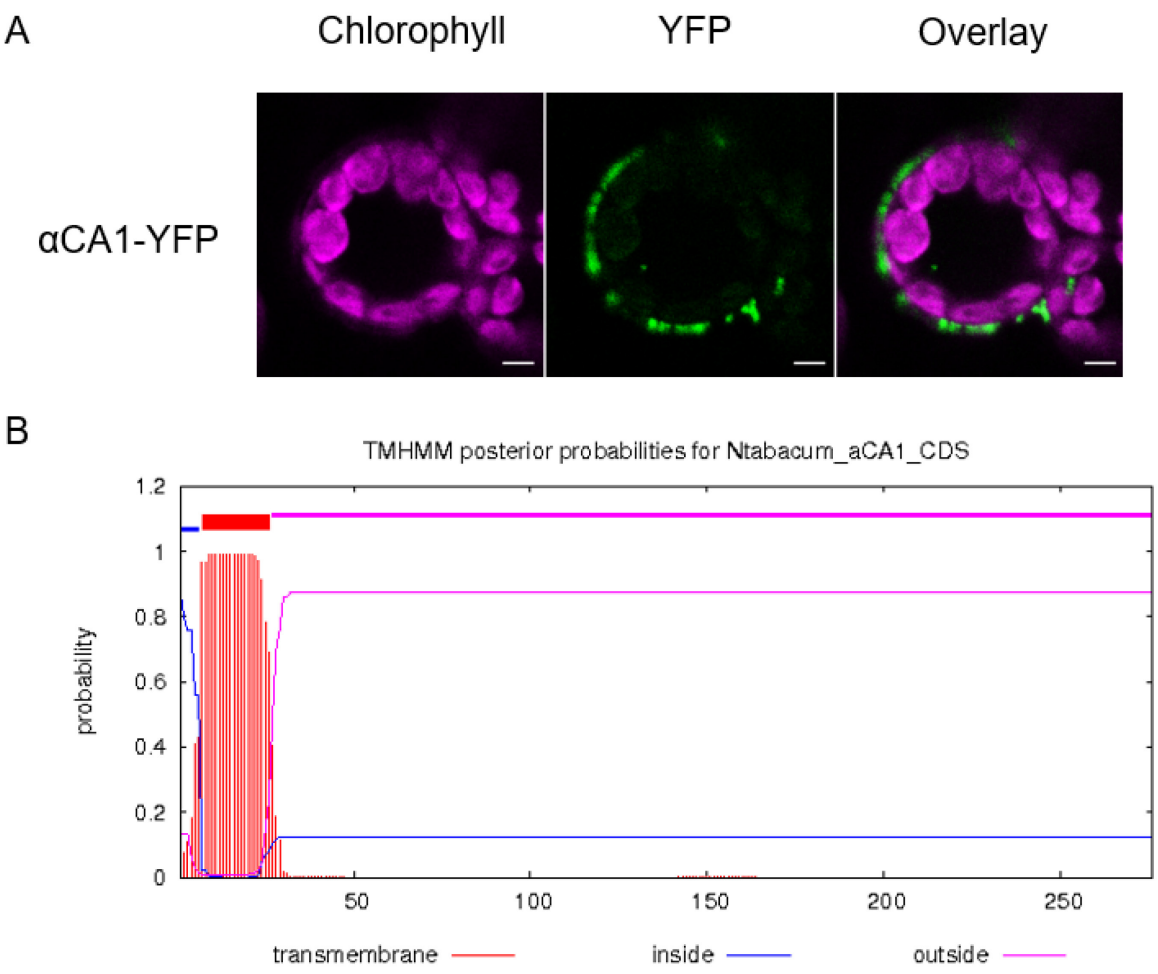

Fig. S1. (A) αCA1-YFP is not found in the chloroplast stroma and appears to be located on the plasma membrane. Bars=5 µm (B) TMHMM Server v. 2.0 prediction of αCA1 (accession XP_016483347) showing a transmembrane domain and peptide locations. Supports Fig. 2

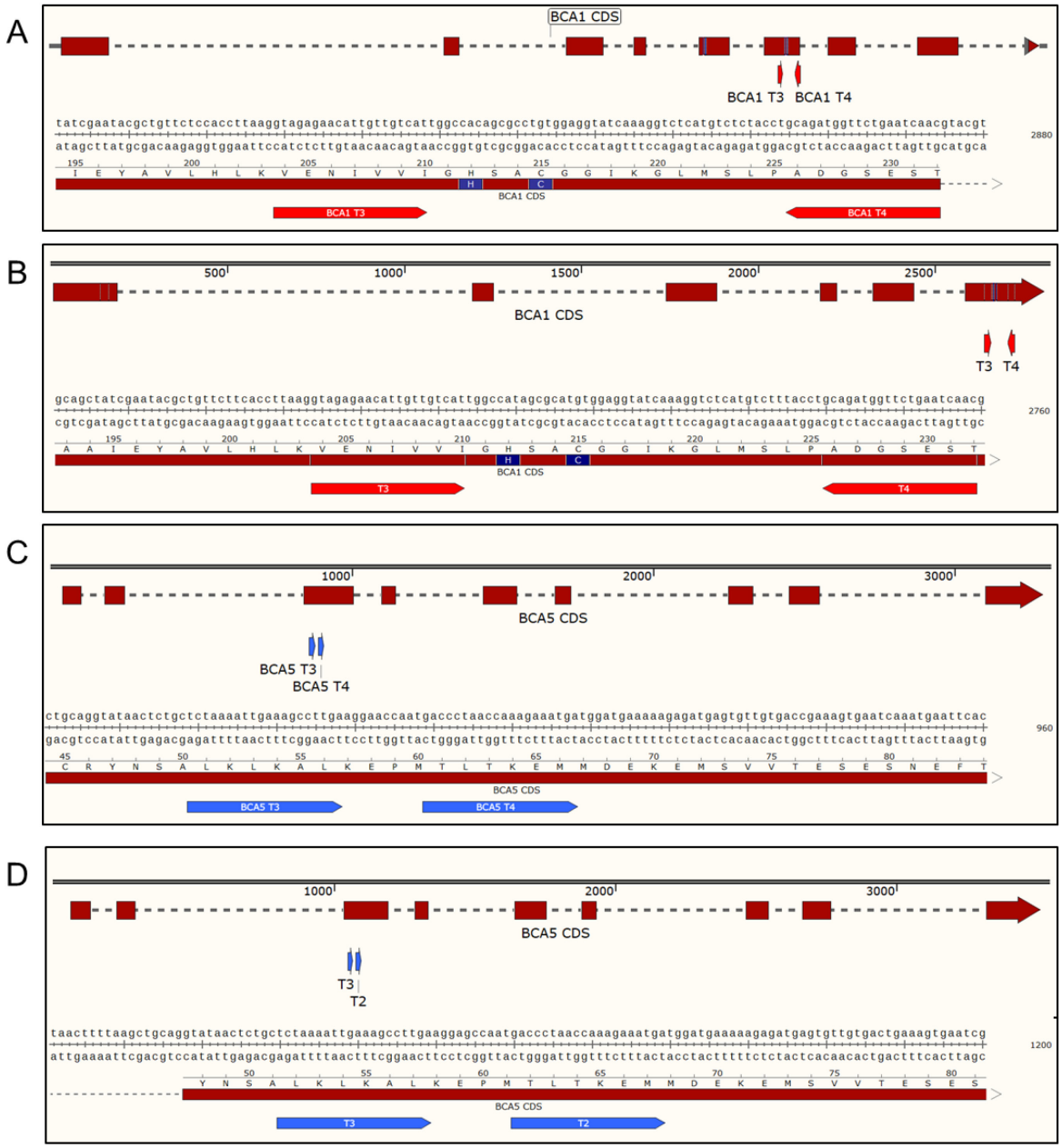

Fig. S2 sgRNA targeting sites for βCA1 and βCA5 (red). βCA1 coding sequence most similar to *N. sylvestris* (A) and *N. tomentosiformis* (B), with zinc-binding residues shown in blue. βCA5 CDS most similar to *N. sylvestris* (C) and *N. tomentosiformis* (D). Images made with SnapGene. Supports Fig. 2.

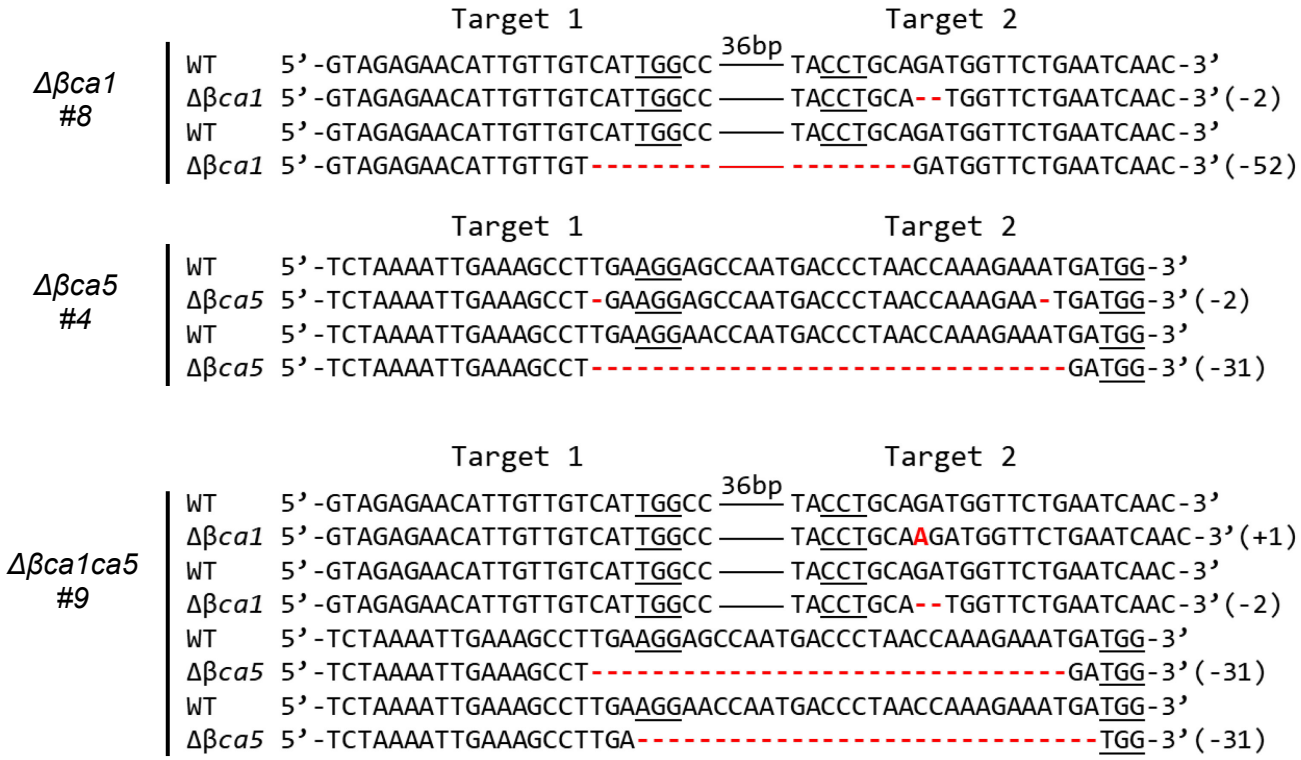

Fig. S3. Sequencing reaction results from T0 generation mutant lines created through the CRISPR/Cas9 system. Parentheses indicate the net change in the nucleotide number between CA mutant homologs and the respective WT mRNA sequence. PAM sequences of each target are underlined. Sequence changes are indicated in red. Supports Fig. 2.

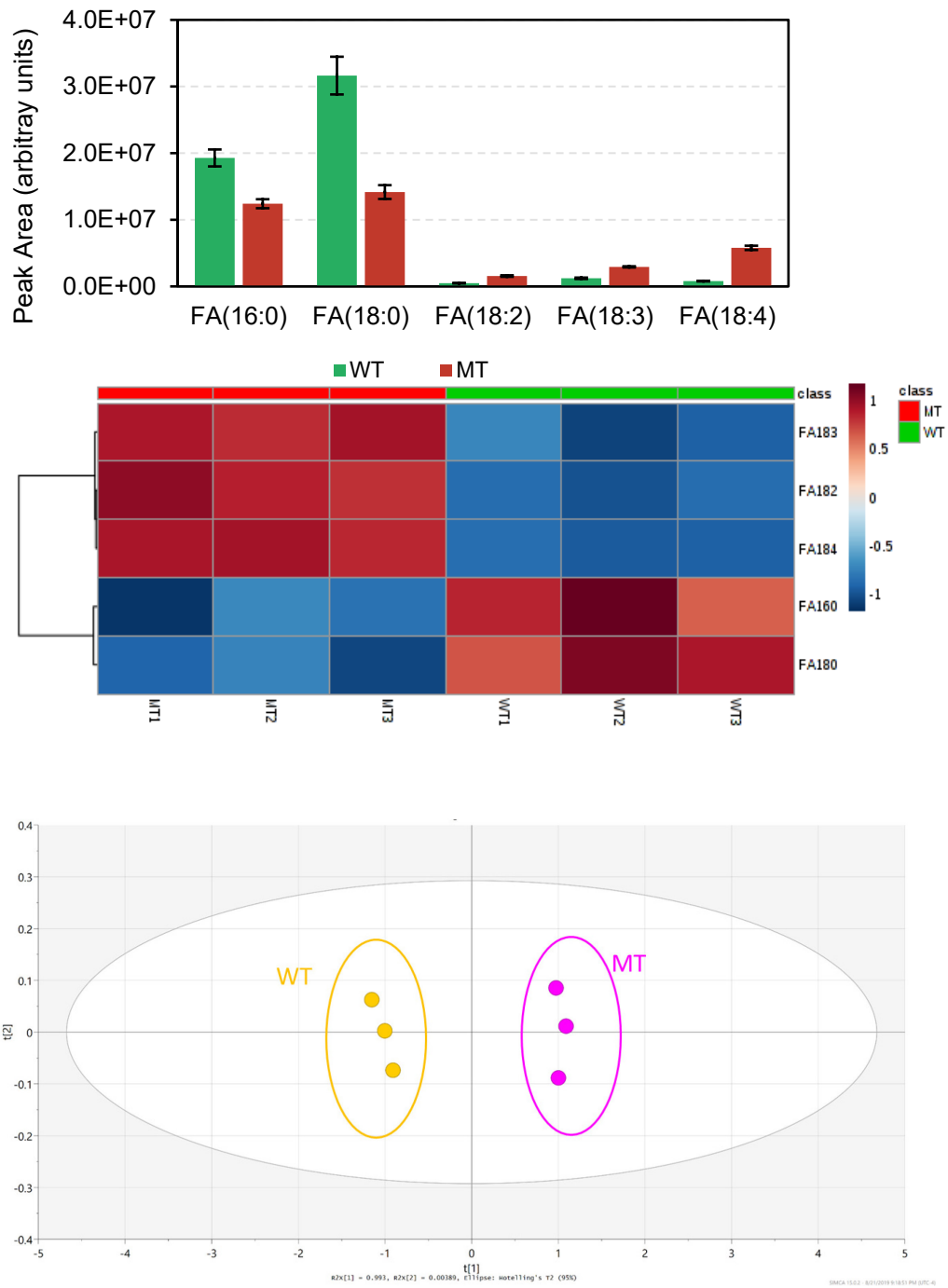

Fig. S4. Free fatty acid analysis. (A) Peak area of WT and Δβ*ca1ca5* (MT) FFAs normalized with an internal standard (heptadecanoic acid). Multivariate analysis showed clear differences between WT and Δβ*ca1ca5* based on FFA analysis as seen in (B) Heat map of individual replicates using metaboanalyst data and (C) Principal component analysis score plot: Log transform and Pareto scale. Supports Fig. 4A.

A

3 days post transfer to ambient CO_2

6 days post transfer to ambient CO_2

B

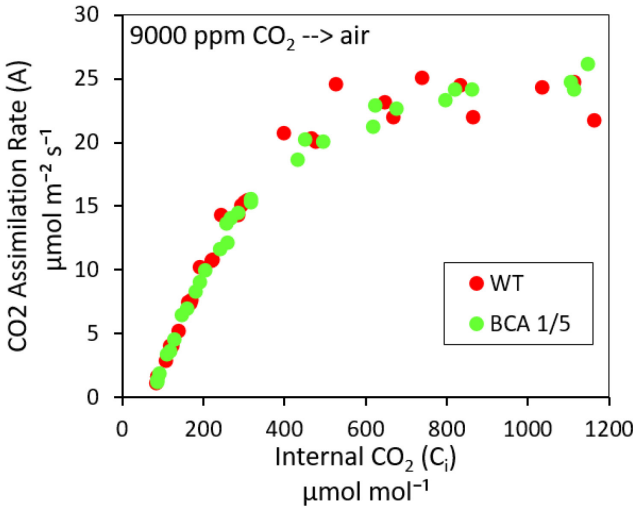

C

Condition/Figure	g_m for WT µmol m^{-2} s^{-1} Pa^{-1}	g_m for Δβca1ca5 µmol m^{-2} s^{-1} Pa^{-1}
High CO_2 grown/Fig. 5D	1.77 ± 0.32	1.64 ± 0.28
Ambient adapted/Fig.S5	1.59 ± 0.14	1.52 ± 0.06

Fig. S5: Photosynthetic measurements in ambient conditions. WT and *Δβca1ca5* grown in high CO_2 were transferred to allow growth in air. (A) At 72 hours, the bicarbonate deficiency phenotype was clearly visible in developing leaves of the *Δβca1ca5* (red arrow). This visual phenotype was not visible in fully matured leaves of *Δβca1ca5* even after 6 days at ambient CO_2 (blue arrow). (B) A/C_i curves of fully matured leaves from plants transferred to air for at least 72 hours were obtained (3 leaves from 2 plants for each genotype). The blue arrow points to an example of the type of leaf that was assayed. (C) Mesophyll conductance (g_m) was estimated from the A/Ci curve data using the calculator described by Sharkey, PCE 2015 (7). Supports Figure 5.

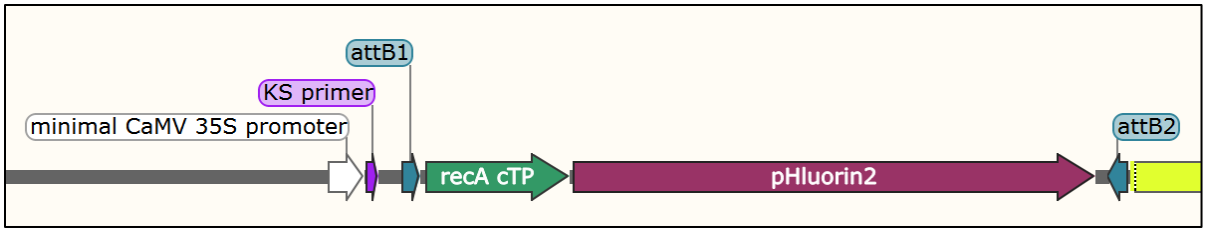

Fig. S6. Diagram of the construct map of the pHluorin2 expression plasmid showing the Arabidopsis RecA chloroplast transit peptide (at the N-terminus). Supports Fig. 6.

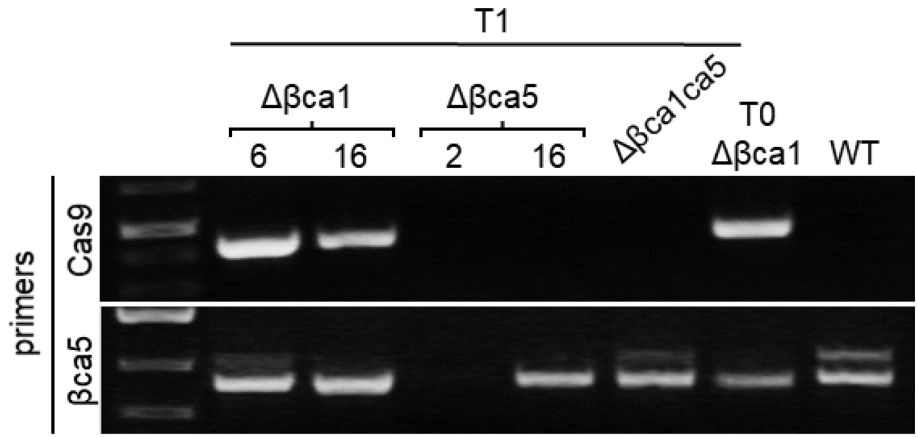

Fig. S7. PCR (using gDNA template) of selected T1 plants (numbered) generated by self pollination shows an absence of the CRISPR/Cas9 gene cassette in *Δβca1ca5*. This T1 *Cas9- Δβca1ca5* plant was used in the complementation experiments. Supports Fig. 8

Primer	5'-3' Sequence	Purpose
SpeI dcTP_BCA1_For	CGCACTAGTATGGAAGAAATGGCTA ACGAATCC	Remove cTP from βca1
BCA1_CA-DA For	CTGCCTCACGAGTGTGCCCATC	Q5 mutagenesis of zinc binding sites
BCA1_CA-DA Rev	AGGCGGCAAAGACCATGTACTTG	Q5 mutagenesis of zinc binding sites
BCA1_gRNA3_BsaI f	TGTGGTCTCAATTGTAGAGAACATT GTTGTCATGTTTTAGAGCTAGAAATA GCAAG	Create gRNA for βca1 off of pICH86966::AtU6p::sgRNA_PDS plasmid
BCA1_gRNA4_BsaI f	TGTGGTCTCAATTGTTGATTCAGAAC CATCTGCGTTTTAGAGCTAGAAATA GCAAG	Create gRNA for βca1 off of pICH86966::AtU6p::sgRNA_PDS plasmid
BCA5_gRNA3_BsaI f	TGTGGTCTCAATTGCTAAAATTGAAA GCCTTGAGTTTTAGAGCTAGAAATA GCAAG	Create gRNA for βca5 off of pICH86966::AtU6p::sgRNA_PDS plasmid
BCA5_gRNA4_BsaI f	TGTGGTCTCAATTGACCCTAACCAA AGAAATGAGTTTTAGAGCTAGAAATA GCAAG	Create gRNA for βca5 off of pICH86966::AtU6p::sgRNA_PDS plasmid
pICH_bsa_FWD	AGGCACAGGTCTCGGGAGTGATCA AAAGTCCCACATCG	Adds RE sites to PCR product off of pICH86966
pICH_bsa_REV	AGGCACAGGTCTCGAGCGAAAAAAA GCACCGACTCG	Adds RE sites to PCR product off of pICH86967
pHlourin2-For	ATGGTGAGCAAGGGCGA	Amplifying pHlourin2 off pME plasmid
pHl2-Rev-EcoR1	ATTACGGAATTCGCCCTTTCACTTGT ACAG	Amplifying pHlourin2 off pME plasmid. Adds EcoRI RE site
CTP-for-EcoR1	CATGGCGAATTCATGGATTCACAGC TAGTCTTGTCTCTG	Amplifying RecA transit peptide. Adds EcoRI RE site
CTP-pHl2-R1	TCGCCCTTGCTCACCATGTCGCGAT CGAACTCAG	Amplifying RecA transit peptide. Aligns with pHlourin2-For and removes EcoRI site

Table S1. Names and sequences of the primers used in the generation of plasmids for stable and transient transformation of tobacco. CRISPR Guide RNA target sequence is underlined.

References

1. I. A. Sparkes, J. Runions, A. Kearns, C. Hawes, Rapid, transient expression of fluorescent fusion proteins in tobacco plants and generation of stably transformed plants. *Nat Protoc* **1**, 2019-2025 (2006).
2. C. Engler, R. Kandzia, S. Marillonnet, A one pot, one step, precision cloning method with high throughput capability. *PloS one* **3**, e3647 (2008).
3. C. Engler, R. Gruetzner, R. Kandzia, S. Marillonnet, Golden gate shuffling: a one-pot DNA shuffling method based on type IIs restriction enzymes. *PloS one* **4**, e5553 (2009).
4. E. Weber, R. Gruetzner, S. Werner, C. Engler, S. Marillonnet, Assembly of designer TAL effectors by Golden Gate cloning. *PloS one* **6**, e19722 (2011).
5. L. Medina-Puche *et al.*, beta-carbonic anhydrases play a role in salicylic acid perception in Arabidopsis. *PloS one* **12**, e0181820 (2017).
6. C. S. Roberts, M. H. Spalding, Post-translational processing of the highly processed, secreted periplasmic carbonic anhydrase of *Chlamydomonas* is largely conserved in transgenic tobacco. *Plant Mol Biol* **29**, 303-315 (1995).
7. T. D. Sharkey, What gas exchange data can tell us about photosynthesis. *Plant, Cell & Environment* **39**, 1161-1163 (2016).
8. H. S. Padgett, Y. Watanabe, R. N. Beachy, Identification of the TMV Replicase Sequence That Activates the *N* Gene-Mediated Hypersensitive Response. *Mol Plant Microbe In* **10**, 709-715 (1997).
9. H. S. Padgett, R. N. Beachy, Analysis of a tobacco mosaic virus strain capable of overcoming *N* gene-mediated resistance. *The Plant Cell* **5**, 577-586 (1993).